Supplementary Information

Red-Light Photoredox Catalysis with Bridged Fluorescein Derivatives: Mechanistic Insights and Application to Fluoride-Responsive Photopolymerization

Dokyeong Lee[a], Ho Yun Kim[a], Byunghyuck Jung[b], Sung Ho Yang[c], Hong-In Lee,*[,a] and Jungkyu K. Lee*[,a]

[a]*Department of Chemistry and Green-Nano Materials Research Center, Kyungpook National University, Daegu 41566, South Korea.*

[b]*Department of Physics and Chemistry, Daegu Gyeongbuk Institute of Science and Technology (DGIST), Daegu 42988, South Korea.*

[c]*Department of Chemistry Education, Korea National University of Education (KNUE), Cheongju 28173, South Korea.*

*To whom correspondence should be addressed.

Email: jkl@knu.ac.kr and leehi@knu.ac.kr

Tel: +82-53-950-5339

Fax: +82-53-950-6330

1. Materials. Fluorescein (> 97.5%, Sigma-Aldrich), 4,5-dibromofluorescein (> 95%, Sigma-Aldrich), eosin Y disodium salt (Alfa Aesar), sulfuric Acid (Duksan Pure Chemicals Co.), methylene chloride (MC, Honeywell Burdick), methanol (Alfa Aesar), ethyl acetate (Daejung Chemicals & metals Co., Ltd.), ethanol (Sigma-Aldrich), oligo(ethylene glycol) methyl ether methacrylate (OEGMA, average M_n = 500 g/mol, Sigma-Aldrich), 2-hydroxyethyl methacrylate (HEMA, 97%, Thermo Fisher), *N*-isopropylacrylamide (NIPAm, TCI), 3-sulfopropyl methacrylate (SPMA, 98%, Sigma-Aldrich), 2-acrylamido-2-methyl-1-propanesulfonic acid sodium salt solution (AMPS, 50 wt. % in H_2O, Sigma-Aldrich), dimethylmalonic acid (98%, Sigma-Aldrich), deuterium oxide (99.90% D, Eurisotop), dimethylsulfoxide-d_6 (99.80% D, Eurisotop), trifluoroacetic acid-*d* (99.50% D, Sigma-Aldrich), sodium hydroxide (NaOH, >93%, Duksan Pure Chemicals Co.), tetrabutylammonium chloride (>97%, Sigma-Aldrich), 5,5-dimethyl-1-pyrroline-*N*-oxide (DMPO, >97%, TCI), lithium bromide (LiBr, >99%, TCI), buffer solution (sodium phosphate dibasic dodecahydrate 7.0–14.0 mM, sodium hydroxide 1.25–12.5 mM, pH 11, Duksan Pure Chemicals Co.), *N*,*N*-dimethylformamide (DMF, HPLC grade, Honeywell Burdick), triethanolamine (TEOA, Sigma-Aldrich), diphenyliodonium hexafluorophosphate (IOD, Sigma-Aldrich), 4-((((2-carboxyethyl)thio)carbonothioyl)thio)-4-cyanopentanoic acid (CTA, **1**, Sigma-Aldrich), *N*,*N*-diethyl-*p*-phenylenediamine sulfate (DPD, Sigma-Aldrich), peroxidase from horseradish (POD, Type II, Sigma-Aldrich), disodium terephthalate (>99%, Alfa Aesar), hydrogen peroxide (28.0%, Duksan Pure Chemicals Co.), 2,2,6,6-tetramethylpiperidine-1-oxyl (TEMPO, 99%, Sigma-Aldrich), *p*-nitrobenzenesulfonyl chloride (>97%, Alfa Aesar), sodium bicarbonate (Alfa Aesar), methylene blue (Sigma-Aldrich), triethylamine (>99%, SAMCHUN), tetrabutylammonium fluoride (TCI), poly(ethylene glycol) diacrylate (PEGDA, average M_n = 575 g/mol, Sigma-Aldrich), 1,8-diazabicyclo[5.4.0]undec-7-ene (DBU, >98%, Sigma-Aldrich), potassium

diamminetetrakis(thiocyanato-*N*) chromate (potassium reineckate, $K[Cr(NH_3)_2(CNS)_4]$) (>93%, Alfa Aesar), iron(III) nitrate nonahydrate (>99%, Sigma-Aldrich), perchloric acid (>70%, Sigma-Aldrich), red LED (wavelength: 660 ± 30 nm, 5.9 W/cm^2, QB4675-50W, luminous flux: 5500-6000), near-IR (NIR) LED (wavelength: 730 ± 30 nm, 12.5 W/cm^2), and deionized water (water, 18.2 MΩ·cm, Milli-Q® Direct Water Purification System, Merck Millipore) were purchased and used without further purification.

2. Experimental procedures and details.

Synthesis of 7-hydroxynaphtho[3,2,1-kl]xanthene-3,9-dione (coerulein B, CB). Fluorescein (100 mg, 0.301 mmol) was dissolved in concentrated H_2SO_4 (10 mL) and stirred at 180 °C for 24 h under an argon atmosphere. After cooling to room temperature, the reaction mixture was slowly poured into ice-cold water and allowed to stand at 4 °C for 24 h. The resulting precipitate was collected by centrifugation and washed three times with water and methanol. The crude solid was purified by column chromatography on silica gel using CH_2Cl_2/MeOH (20:1 → 5:1) as the eluent. The purified product was then dried under reduced pressure to afford **CB** as a black solid (30 mg, 31.7%). ^{1}H NMR (700 MHz, trifluoroacetic acid-*d*): δ 8.87-8.85 (d, 1H, J = 9.3 Hz), 8.72-8.70 (m, 1H), 8.57-8.55 (m, 1H), 8.38 (d, 1H, J = 2.3 Hz), 8.15 (m, 2H), 7.76 (d, 1H, J = 2.3 Hz), 7.72-7.70 (dd, 1H, J = 9.4 and 2.4 Hz), 7.67 (d, 1H, J = 2.3 Hz) (Fig. S1).

Synthesis of 4,6-dibromo-7-hydroxynaphtho[3,2,1-kl]xanthene-3,9-dione (BBF). 4′,5′-Dibromofluorescein (200 mg, 0.408 mmol) was dissolved in concentrated H_2SO_4 (15 mL) and stirred at 180 °C for 24 h under an argon atmosphere. After cooling to room temperature, the reaction mixture was slowly poured into ice-cold water and allowed to stand at 4 °C for 24 h.

The resulting precipitate was collected by centrifugation and washed three times with water and methanol. The crude solid was purified by silica column chromatography using MC/MeOH (15:1 → 3:1) as the eluent. The purified product was dried under reduced pressure to afford **BBF** as a black solid (100 mg, 52.2%). ^{1}H NMR (700 MHz, trifluoroacetic acid-*d*): δ 8.87-8.85 (d, 1H, *J* = 9.5 Hz), 8.70-8.69 (dd, 1H, *J* = 7.5 and 1.4 Hz), 8.53-8.52 (d, 1H, *J* = 7.4 Hz), 8.45 (s, 1H), 8.19-8.16 (m, 1H), 8.15-8.13 (m, 1H), 7.86-7.84 (d, 1H, *J* = 9.5 Hz) (Fig. S2); ^{13}C NMR (125 MHz, trifluoroacetic acid-*d*): δ ppm 184.81, 170.48, 167.33, 160.57, 159.00, 156.06, 139.90, 137.90, 137.74, 135.90, 134.50, 133.42, 133.40, 131.53, 123.35, 122.45, 117.82, 116.21, 106.92, 101.72 (Fig. S3); MS (HRMS-FAB): *m*/*z* = 472.8971 $[M+H]^+$ (cal. 472.8847 $[M+H]^+$) (Fig. S4).

Synthesis of 2,4,6-tribromo-3,9-dihydroxynaphtho[3,2,1-kl]xanthene-7,8-dione (BEY). Eosin Y (200 mg, 0.308 mmol) was dissolved in concentrated H_2SO_4 (10 mL) and stirred at 180 °C for 18 h under an argon atmosphere. After cooling to room temperature, the reaction mixture was slowly poured into ice-cold water and allowed to stand at 4 °C for 24 h. The resulting precipitate was collected by centrifugation and washed three times with water and methanol. The crude solid was purified by silica column chromatography using MC/MeOH (10:1 → 2:1) as the eluent. The purified product was dried under reduced pressure to afford **BEY** as a black solid (80 mg, 45.9%). ^{1}H NMR (700 MHz, trifluoroacetic acid-*d*): δ 9.32 (s, 1H), 9.02-9.00 (m, 1H), 8.96-8.95 (d, 1H, *J* = 8.5 Hz), 8.34-8.32 (m, 2H) (Fig. S5).

Synthesis of 3,9-dioxo-3,9-dihydronaphtho[3,2,1-kl]xanthene-7-yl-4-nitrobenzenesulfonate (Sulfonyl-protected CB, 2). CB (50 mg, 0.16 mmol) was dissolved in anhydrous methylene chloride (MC, 50 mL) under an argon atmosphere. Triethylamine (TEA, 1.0 mL, 7.2 mmol) was added at room temperature under continuous stirring. Subsequently, *p*-nitrobenzenesulfonyl chloride (107 mg, 0.48 mmol) was slowly added to the reaction mixture

at 0 °C, and the mixture was stirred at 0 °C for 1 h. After the reaction reached a plateau (monitored by TLC), pure water (30 mL) was added to the reaction mixture at 0 °C. The organic layer was separated, and the aqueous phase was extracted three times with MC (3 × 20 mL). The organic solvent was removed under reduced pressure. The resulting residue was purified by silica gel column chromatography using MC and ethyl acetate (10:1 → 5:1, v/v) as the eluent. The crude mixture was washed with saturated sodium bicarbonate (aq) and stirred for 2 h to remove residual *p*-nitrobenzenesulfonic acid derivatives. The sulfonyl-protected **CB** (**2**) was obtained as a dark red solid. (42 mg, 57.6%).^{1}H NMR (700 MHz, $CDCl_3$): δ 8.49 (d, 1H, J = 7.6 Hz), 8.45-8.43 (d, 2H, J = 9.0 Hz), 8.16 (d, 3H, J = 8.7 Hz), 8.08 (d, 1H, J = 9.9 Hz), 7.88-7.81 (m, 2H), 7.76 (d, 1H, J = 2.4 Hz), 7.48 (d, 1H, J = 2.3 Hz), 6.87-6.85 (d, 1H, J = 9.8 Hz), 6.5 (d, 1H, J = 1.8 Hz) (Fig. S6). ^{13}C NMR (125 MHz, $CDCl_3$): δ ppm 167.72, 133.41, 132.86, 132.64, 132.46, 132.33, 131.69, 131.34, 130.92, 130.42, 130.34, 130.09, 129.89, 129.40, 128.85, 124.81, 117.01, 116.57, 114.76, 107.86 (Fig. S7); MS (HRMS-FAB): m/z = 500.0438 $[M+H]^+$ (cal. 500.0435 $[M+H]^+$) (Fig. S8).

Red-light-induced photo-RAFT polymerization. Photo-RAFT polymerization was carried out in mixed solvent systems containing 50% DMSO (aq), with the total reaction volume adjusted to 0.6 mL. The reaction solution typically consisted of BFL (0.1 mM), OEGMA (250 mM) and CTA (**1**) (1.25 mM). The mixture was transferred into a standard NMR tube and vortexed for 1 min prior to irradiation. Polymerization was then initiated under ambient conditions using a red LED source. After each designated irradiation interval, the reaction mixture was vortexed again and analyzed by ^{1}H NMR and GPC.

Red-light or NIR-induced free-radical polymerization. Photopolymerization was carried out in mixed solvent systems containing 50% DMSO (aq), with the total reaction volume adjusted to 0.6 mL. The reaction solution typically consisted of BFL (0.1 mM), OEGMA (250

mM), and a co-initiator (100 mM). The mixture was transferred into a standard NMR tube and vortexed for 1 min prior to irradiation. Polymerization was then initiated under ambient conditions using either a red LED source or a NIR LED source (730 ± 30 nm, 12.5 $W \cdot cm^{-2}$). After each designated irradiation interval, the reaction mixture was vortexed again and analyzed by ^{1}H NMR and GPC.

Polymerization kinetics using nuclear magnetic resonance (NMR) spectroscopy. For kinetic measurements, ^{1}H NMR spectra were acquired on a Spinsolve 80 MHz spectrometer (Magritek) with 32 scans per run. Monomer conversion was determined by comparing the integrated vinyl proton resonances of OEGMA (δ = 5.5–6.3 ppm) with the methyl proton signal of dimethylmalonic acid (δ = 1.29 ppm), which served as an internal reference (Fig. S43–S48). Prior to red LED irradiation, each reaction mixture was vortexed for 1 min, and the polymerizations were conducted under an ambient atmosphere. For polymerization conducted under an argon atmosphere, the reaction solution in a rubber-sealed vial was purged with argon for 1 h in the dark and then carefully transferred to a J-Young NMR tube inside an argon-filled glovebox. The valve of the NMR tube was sealed to prevent air exposure prior to measurement. For oxygen-rich conditions, the reaction solution in a rubber-sealed vial was purged with oxygen for 1 h in the dark and then carefully transferred to a J-Young NMR tube which was filled with oxygen. The resulting NMR tube was further purged with oxygen to ensure oxygen saturation until analysis.

Photobleaching study. Under ambient conditions, a 50% DMSO (aq) solution containing BFL (0.1 mM) with either CTA (**1**) (1.25 mM) or a co-initiator (100 mM) was prepared in a vial to a total volume of 5 mL. A 500 µL aliquot of the reaction mixture was transferred into a quartz cuvette (Hellma®) and placed onto the LED source. After each irradiation period, the cuvette was gently vortexed three times to ensure thorough mixing. As a negative control, a separate

500 μL aliquot was stored in the dark and analyzed under identical conditions. For argon- and oxygen-rich conditions, the mixture solution (10 mL) in a rubber-sealed vial was purged with the respective gas for 1 h in the dark and then subjected to irradiation. A 500 μL aliquot of the resulting solution was transferred to a quartz cuvette for measurement, and the sample in the cuvette was discarded after each measurement. To maintain the desired atmosphere, a balloon filled with the corresponding gas was attached to the sealed vial throughout the experiment.

Stern-Volmer analysis. Quantitative quenching rate constants were determined by Stern-Volmer analysis. Because TEOA exhibited superior photocatalytic performance compared with the other co-initiators, we investigated the quenching behavior between the BFLs and TEOA in 50% DMSO (aq) under ambient conditions using fluorometry (FP-8700, Jasco). Specifically, a screw-capped cuvette containing BFL (10 μM) and varying concentrations of TEOA was irradiated with the red-light LED for 10 s under ambient conditions, and the fluorescence intensity (I) was then recorded. The measurement parameters were as follows: excitation at 620 nm, emission at 730 nm, and PMT 500 for **BEY**; excitation at 615 nm, emission at 730 nm, and PMT 550 for **BBF**; excitation at 605 nm, emission at 730 nm, and PMT 600 for **CB**. The initial fluorescence intensity (I_0) was measured for BFLs in 50% DMSO (aq) at pH 11, as the fluorescence intensity of the BFLs is pH-dependent.

DPD–POD assay. Quantitative analysis of hydrogen peroxide production was conducted using a colorimetric method based on *N*,*N*-diethyl-*p*-phenylenediamine sulfate (DPD) and peroxidase (POD), which exhibits a molar absorption coefficient of 21,000 $M^{-1}\cdot cm^{-1}$ at 551 nm and a detection limit in the range of 0.2–0.3 $\mu g\cdot L^{-1}$.[1] BFL was added into a vial containing 0.3 mL of phosphate buffer (pH 6.0), 15 μL of DPD (10 $mg\cdot mL^{-1}$ in water) and 15 μL of POD (1 $mg\cdot mL^{-1}$ in water). The final concentration of the BFL was 0.1mM with a total volume of 3.0 mL. The resulting solution was irradiated for 10 min. The calibration curve for the DPD–POD assay

using hydrogen peroxide (up to 15 μM) exhibited a molar absorption coefficient of 27,860 $M^{-1} \cdot cm^{-1}$ at 551 nm (Fig. S13).

Determination of light intensity. The photon flux of the light source (red LED, wavelength: 660 ± 30 nm, 5.9 W/cm^2) was determined by standard Reinecke's salt actinometry.[2] A 10 mM aqueous solution of $K[Cr(NH_3)_2(NCS)_4]$ was prepared in 0.05 M H_2SO_4 and transferred to a quartz cuvette (the optical path length of the cuvette: 1 cm). The solution was irradiated with a 660 nm LED light for 120 s under ambient conditions. After irradiation, 1.5 mL of the analytical reagent consisting of 0.1 M $Fe(NO_3)_3$ and 0.5 M $HClO_4$ (1:1 mixture) was added to the irradiated solution, and the mixture was kept in the dark for 10 min to complete the formation of the $Fe(SCN)^{3+}$ complex. The absorbance of the resulting solution was measured at 450 nm and compared with that of a non-irradiated blank solution (Fig. S26). The difference in absorbance (ΔA = 0.157) was used to calculate the moles of liberated SCN^- according to Equation (1):

$$\text{mol } SCN^- = \frac{V \cdot \Delta A}{l \cdot \varepsilon} \quad (1)$$

$$\text{mol } SCN^- = (0.002 \text{ L} \cdot 0.157)/(1.0 \text{ cm} \cdot 4300 \text{ L} \cdot \text{mol}^{-1} \cdot \text{cm}^{-1}) = 7.3 \times 10^{-8} \text{ mol}$$

Where V is the total volume of the analyzed solution (0.002 L), ε is the molar absorptivity (4300 $L \cdot mol^{-1} \cdot cm^{-1}$), and l is the optical path length of the cuvette. According to the Equation (1), the calculated amount of liberated SCN^- was 7.3×10^{-8} mol. The photon flux was determined by Equation (2). This calculation incorporates the quantum yield of photoaquation of Reinecke's salt (Φ_R) at 660 nm (Φ_R = 0.27, based on the literature), the irradiation time (t =120), and the fraction of light absorbed (f). The value of f (0.18342) was calculated form the measured absorbance (A) at 660 nm via Equation (3). Based on three replicate measurements for accuracy, the photon flux was determined to be 1.37 (±0.15) × 10^{-8} einstein·s^{-1}

Photon flux = (mol SCN^-)/ $\Phi_R \cdot t \cdot f$ (2)

The fraction of light absorbed (f) = $1–10^{-A}$ (3)

Determination of reaction quantum yield (Φ_{rxn}). The reaction quantum yield was determined using Equation (4), where $mol_{product}$ is the moles of product formed at the specific irradiation time, t is the irradiation time, and f is the fraction of light absorbed by photocatalyst ($f > 0.999$).

$\Phi_{rxn} = (mol_{product})/(\text{photon flux} \cdot t \cdot f)$ (4)

Thus, the reaction quantum yield was calculated from the slope of the plot of $mol_{product}$ versus the composite term (photonflux $\cdot$ t $\cdot f$) (Fig. S21).

Determination of initiator efficiency (Φ_i). The initiator efficiency (Φ_i) was determined using the initiation rate (R_i) and the light absorption of the photocatalyst (I_a), as defined by Equation (5). The light absorption of photocatalyst was calculated using the Beer-Lambert law (Equation (6)), where A is the absorbance of the photocatalyst, and I_0 is the incident light. The incident light (I_0) was determined through chemical actinometry, following Equation (7). This calculation uses the rate of loss of an actinometric compound (d[Act]/dt), the quantum yield of actinometric compound ($\Phi_R = 0.27$), and the fraction of light absorbed by the actinometric compound ($f = 0.18342$) as shown in Equation (7).

$\Phi_i = R_i/I_a$ (5)

$I_a = I_0 (1–10^{-A})$ (6)

Based on three replicate measurements for accuracy, the value of I_0 was determined to be 6.85 (± 0.6) $\times 10^{-6}$ $M \cdot s^{-1}$.

$I_0 = – (d[\text{Act}])/(\Phi_R \cdot f \cdot dt)$ (7)

Based on three replicate measurements for accuracy, the calculated values of I_a were determined to be 6.60 (±0.6) × 10^{-7} M·s^{-1} for **BEY** (0.01 mM) with TEOA (0.1 M), 4.35 (± 0.4) × 10^{-6} M·s^{-1} for **BEY** (0.1 mM) with TEOA (0.1 M), and 5.94 (±0.5) × 10^{-6} M·s^{-1} for **BEY** (0.2 mM) with IOD (0.1 M).

3. Characterizations.

UV–Vis and time-resolved luminescence spectroscopy. The excitation spectra for 350 nm–900 nm were obtained using a UV–Vis spectrophotometer (UV-1800, Shimadzu). The emission spectra and lifetimes of the synthesized BFLs (0.1 mM) containing 10 mM NaOH in ethanol were recorded on an FLS1000 fluorescence spectrophotometer (Edinburgh Instruments, UK). Measurements were carried out at room temperature, and fluorescence lifetimes were obtained at 77 K using an agile xenon flash lamp as the excitation source. Phosphorescence spectra and lifetimes were collected at 77 K under gated detection with a microsecond flashlamp. Typical acquisition settings included an excitation wavelength range of 600–620 nm, a dwell time of 1 s per point, a step size of 1 nm, excitation and emission slit widths of 8.0 nm, and a gate delay of 2 ms. Decay curves were analyzed by iterative deconvolution and fitted to the function $I(t) = B_1 \times e^{-t/\tau_1} + B2 \times e^{-t/\tau_2}$ to extract both fluorescence and phosphorescence lifetimes.

Electron paramagnetic resonance (EPR). The room-temperature EPR spectra were recorded using a Bruker EMSplus–9.5/2.7 spectrometer. Each sample was prepared by dissolving **BEY** (1 mM) in 50% DMSO (aq) containing 0.1 M DMPO and either 0.1 M CTA (**1**) or 0.1 M co-initiator. The solution was irradiated with red light for different time intervals under ambient conditions to monitor the generation and evolution of radical intermediates. Following

irradiation, the reaction mixture was carefully transferred into a glass capillary tube prior to EPR measurement. EPR experimental conditions were as follows: microwave frequency, 9.428–9.412 GHz; microwave power, 6.32 mW; modulation amplitude, 1 G; modulation frequency, 100 kHz; time constant, 81.92 ms; and scan speed, 97.7 G/min.

Gel permeation chromatography (GPC). GPC was performed in DMF containing 1 mM LiBr at a flow rate of 1.0 $mL \cdot min^{-1}$ using a Shimazu chromatograph equipped with a guard column (OHpak SB-G 6B, Shodex) and two main columns (OHpak SB-806NHQ, 300 mm × 8.0 mm) connected in series. A Shimadzu's Nexera system equipped with a refractive index detector (RID-20A) and an autosampler were used. The system was calibrated with polymethylmethacrylate (PMMA) standards (Shodex).

Electrochemical Measurement. The electrochemical properties of the bridged fluoresceins (BFLs) were examined using a three-electrode setup composed of a glassy carbon working electrode (diameter = 2 mm), an Ag/AgCl reference electrode (3 M KCl), and a graphite counter electrode. Linear sweep voltammetry (LSV) was carried out with a PGSTAT128N potentiostat (Autolab) controlled by the Nova 2.1 software package. For measurements, solutions of each BFLs (1 mM) were prepared in a 50% DMSO containing 10 μM NaOH (aq). Analogous solutions of TEOA (1 mM), IOD (1 mM) and CTA (**1**) (1 mM) were also made in the same solvent system. All samples were thoroughly degassed with argon prior to recording. The resulting LSV curves for BFLs, CTA (**1**), IOD and TEOA are shown in the Figs. S29, 30, 32, and 33, and the corresponding half-wave reduction potentials ($\mathbf{E^{red}_{1/2}}$) for their respective redox processes are summarized.

Mass spectroscopy. High-resolution mass spectrometry (HRMS) was carried out using a JEOL JMS-700 spectrometer (ionization mode: fast-atom bombardment (FAB)) at the Korea Basic Science Institute (Daegu).

4. Supporting figures

Scheme S1 Plausible synthetic mechanisms for synthesis of bridged fluorescein derivatives: (a) **CB** and **BBF**; (b) **BEY**.

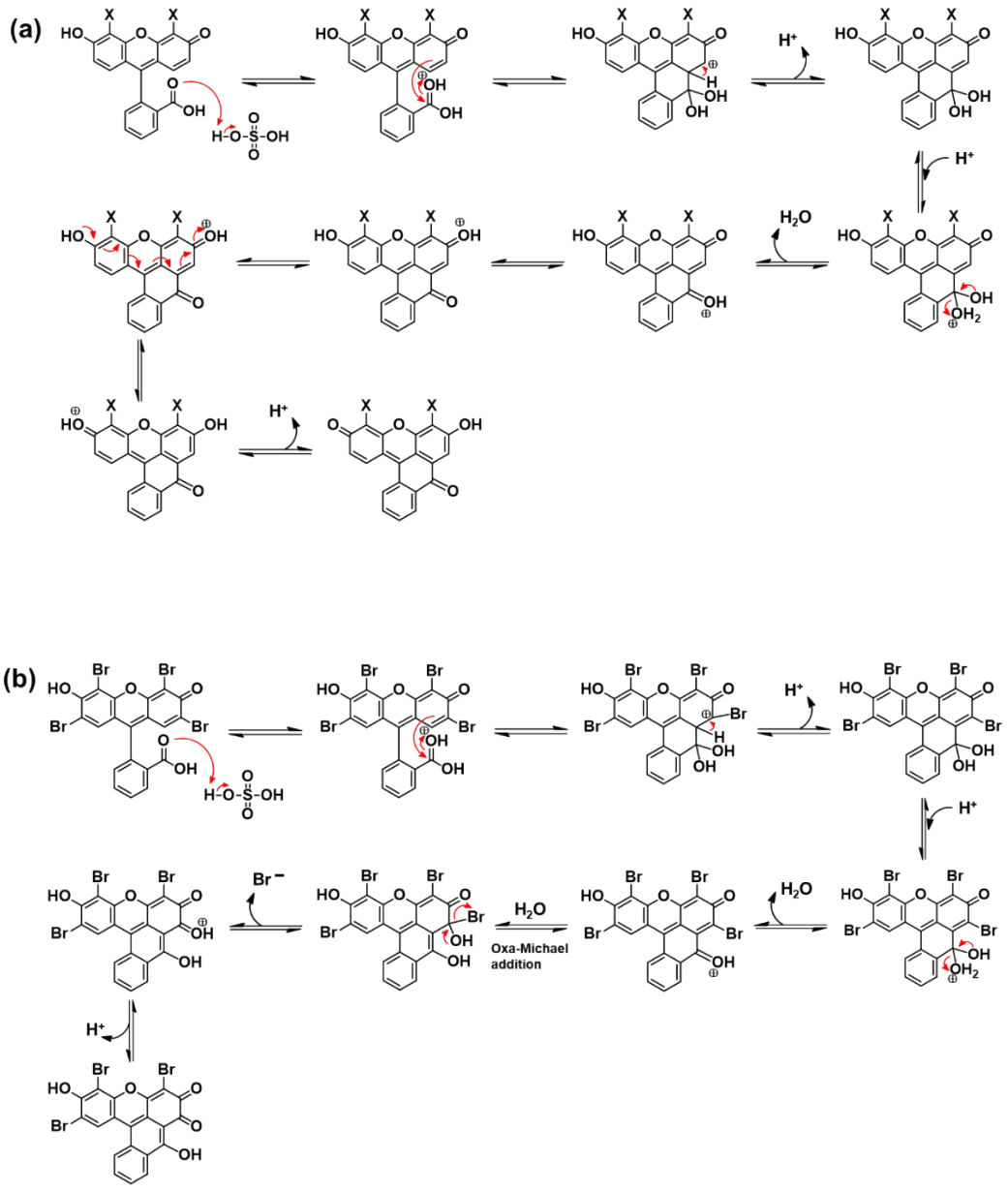

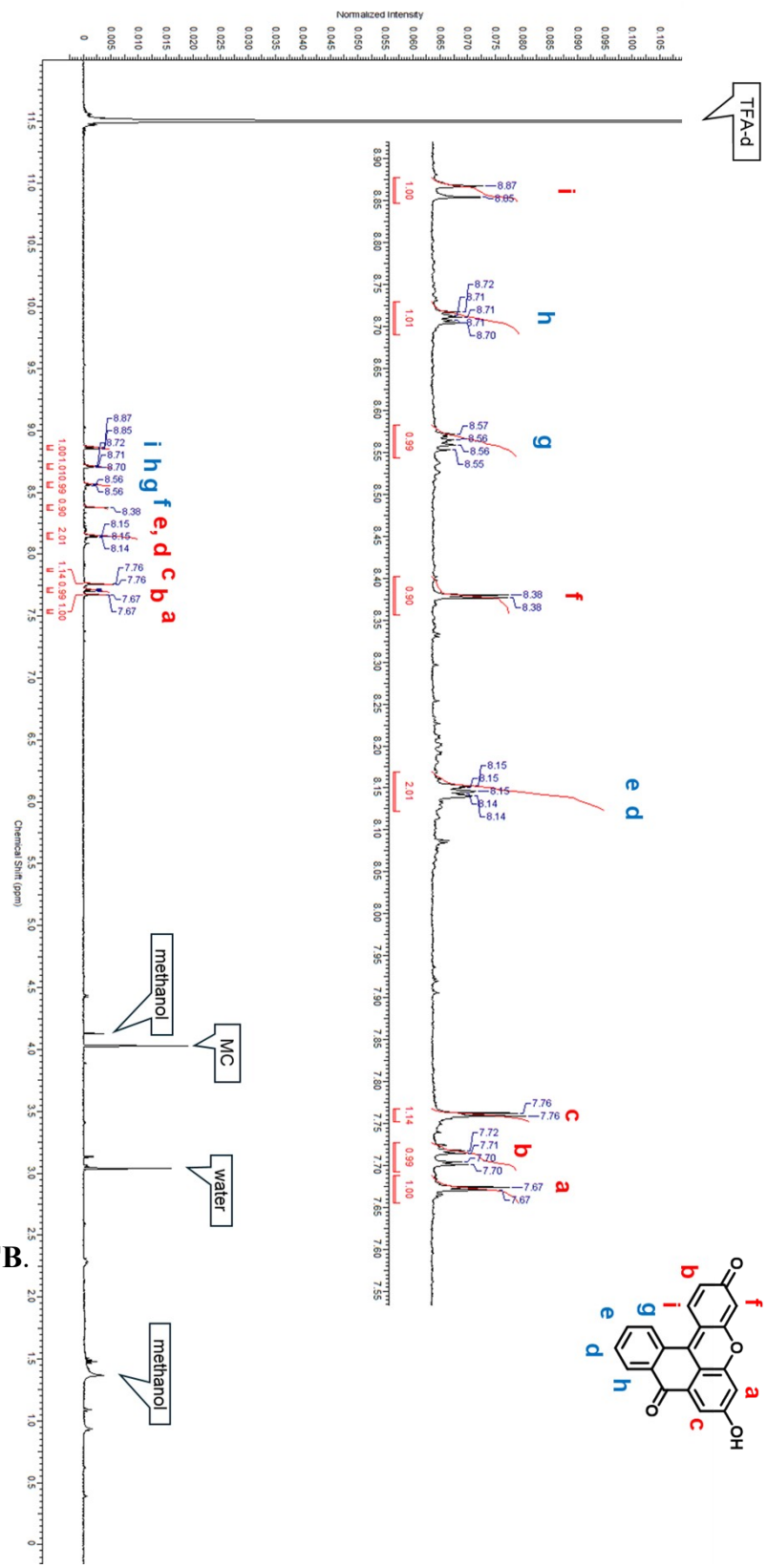

Fig. S1 ^{1}H NMR spectrum of **CB**.

Fig. S2 ^{1}H NMR spectrum of **BBF**.

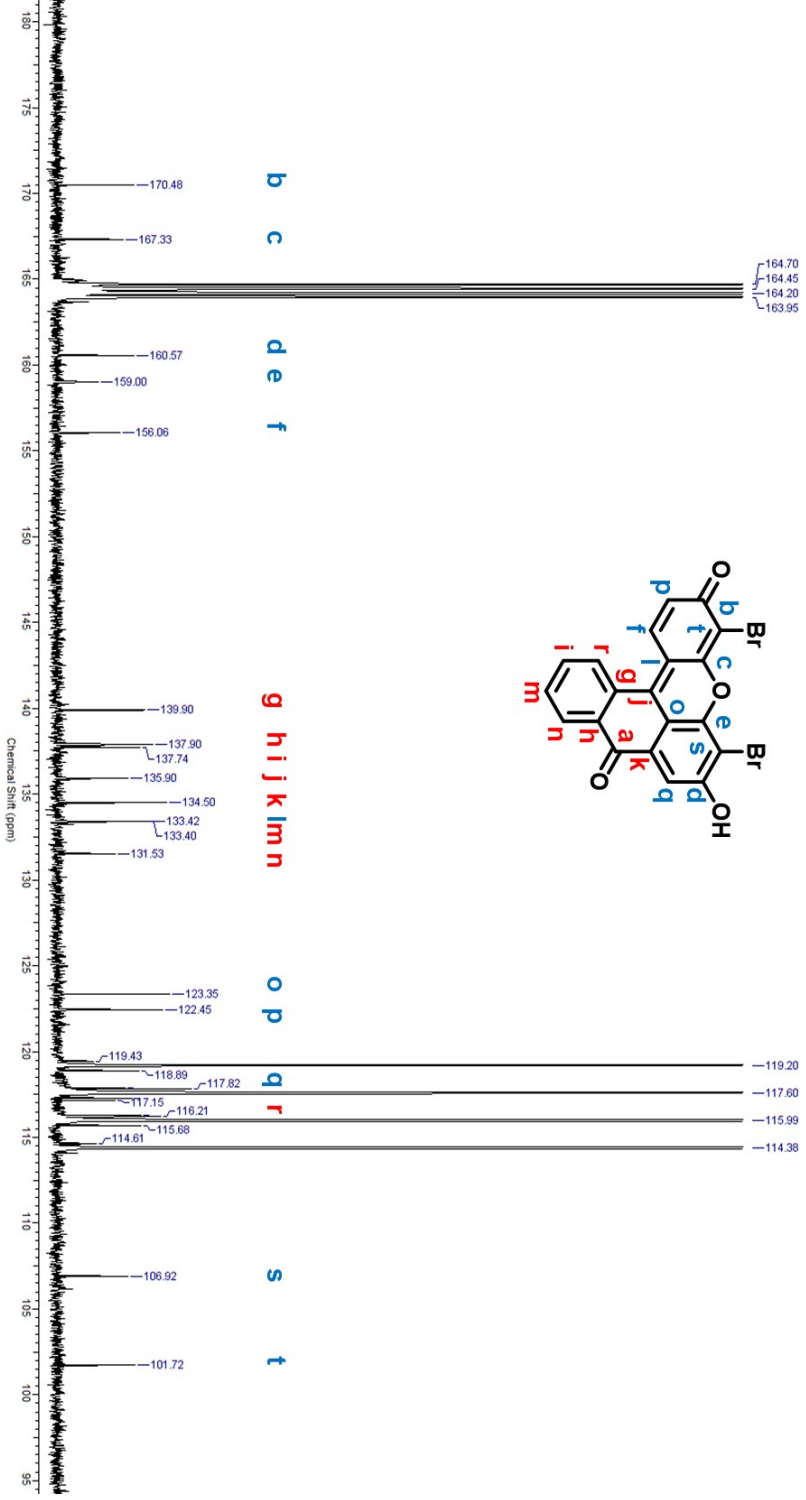

Fig. S3 ^{13}C NMR spectrum of **BBF**.

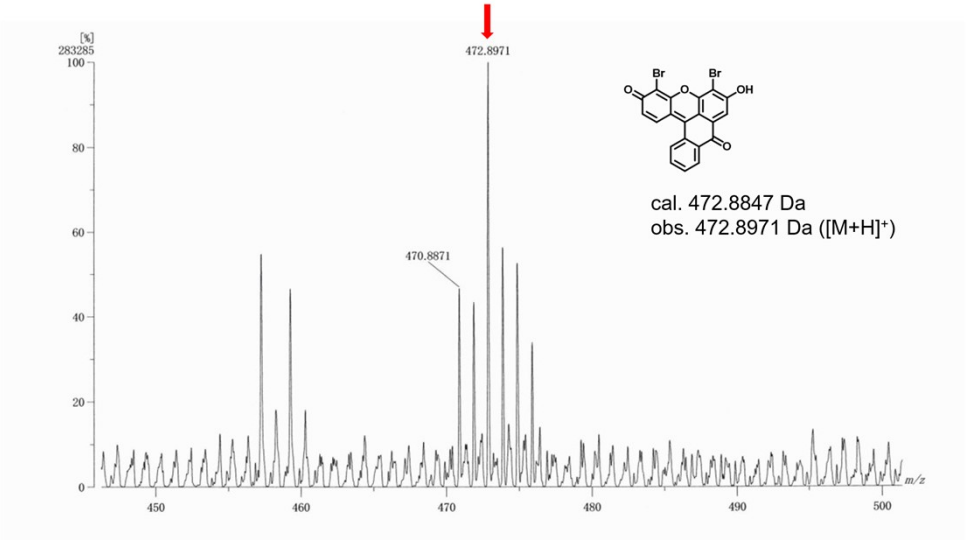

Fig. S4

High-resolution fast atom bombardment (HRFAB) mass spectrum of **BBF**.

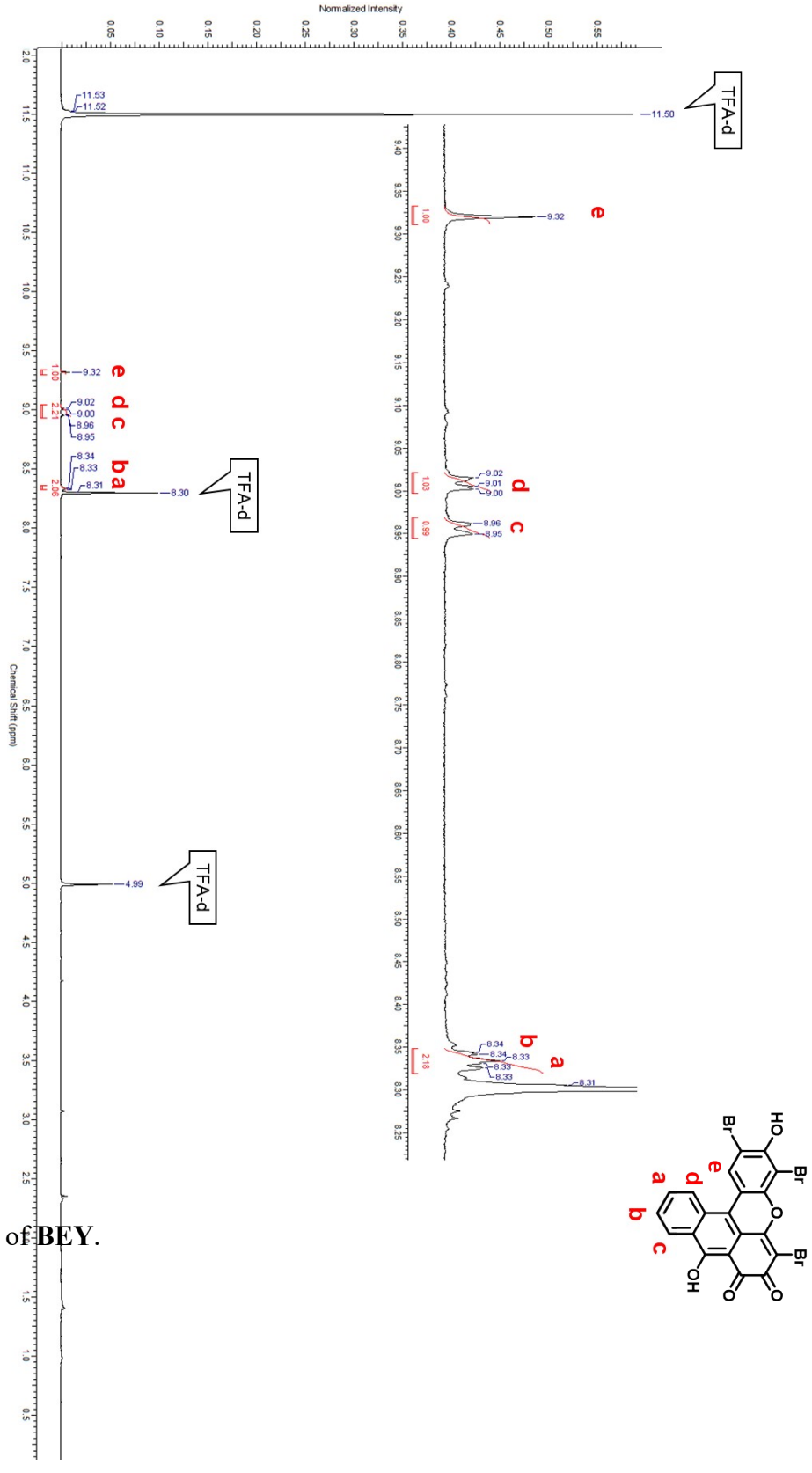

Fig. S5 ^{1}H NMR spectrum of **BEY**.

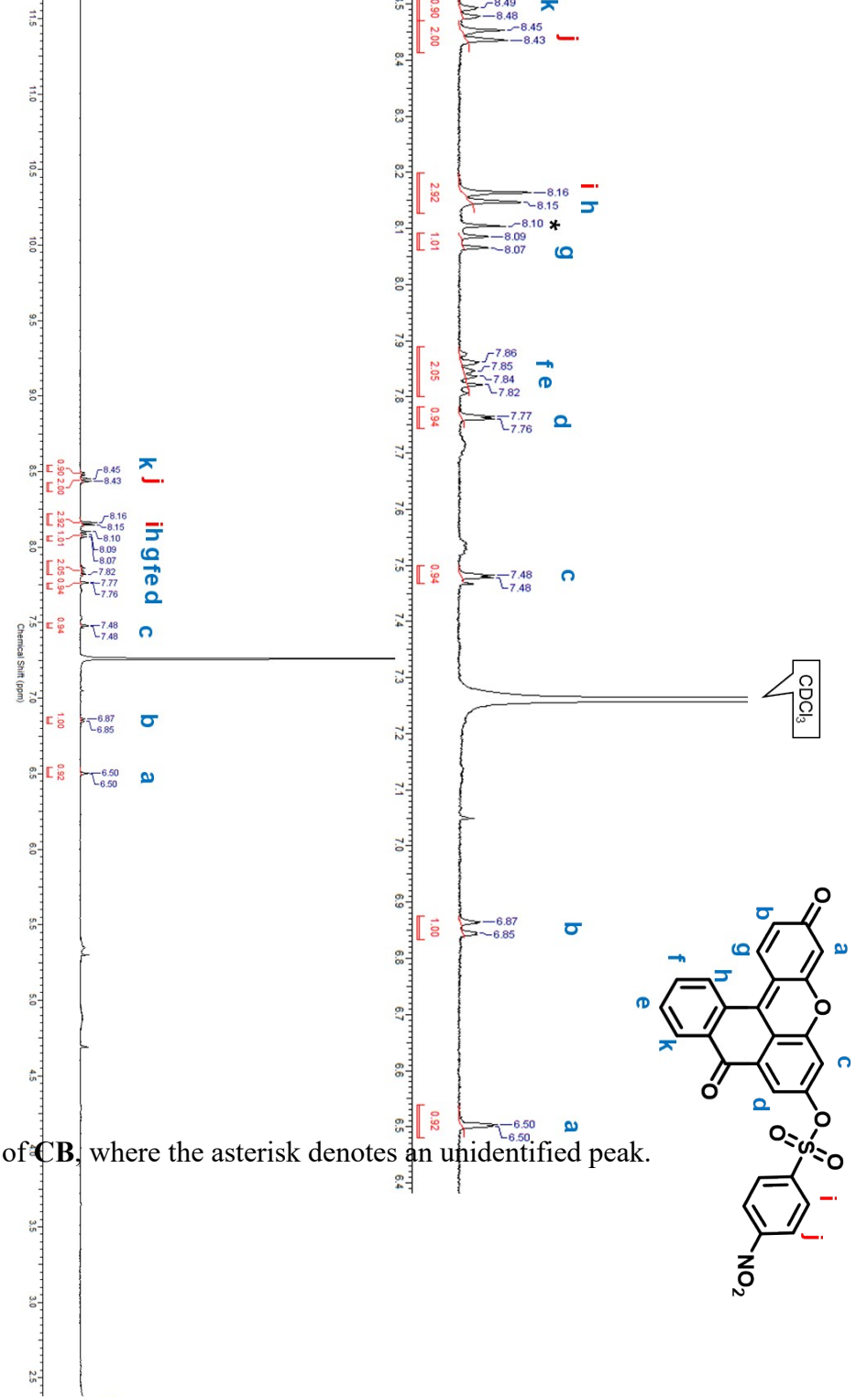

Fig. S6 ^{1}H NMR spectrum of **CB**, where the asterisk denotes an unidentified peak.

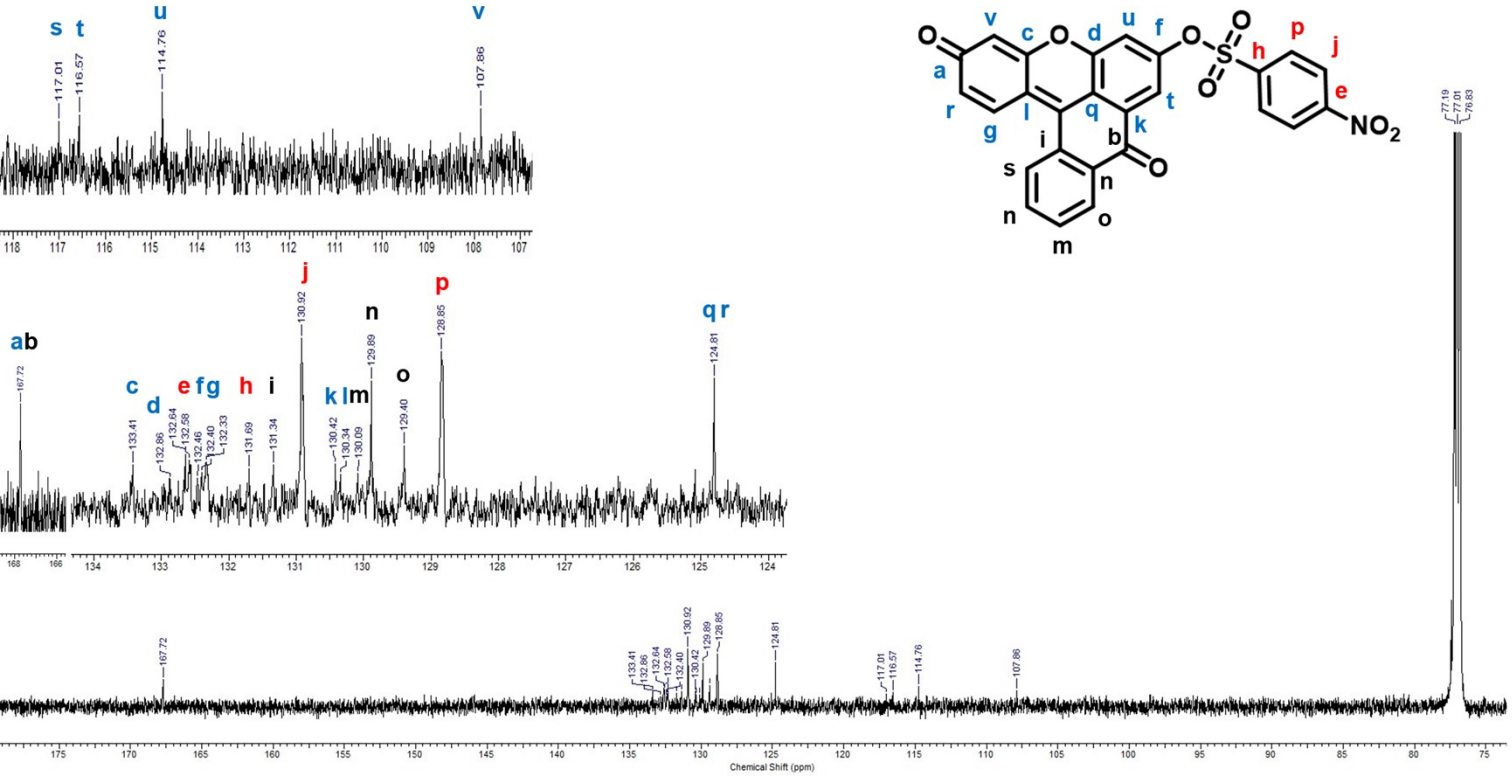
s t u v
117.01
116.57
114.76
107.86
ab
167.72
c d e f g h i j k l m n o p q r
133.41
132.86
132.64
132.58
132.46
132.40
132.33
131.69
131.34
130.92
130.42
130.34
130.09
129.89
129.40
128.85
124.81
77.19
77.01
76.83
Chemical Shift (ppm)

Fig. S7 ^{13}C NMR spectrum of sulfonyl-protected **CB (2)**.

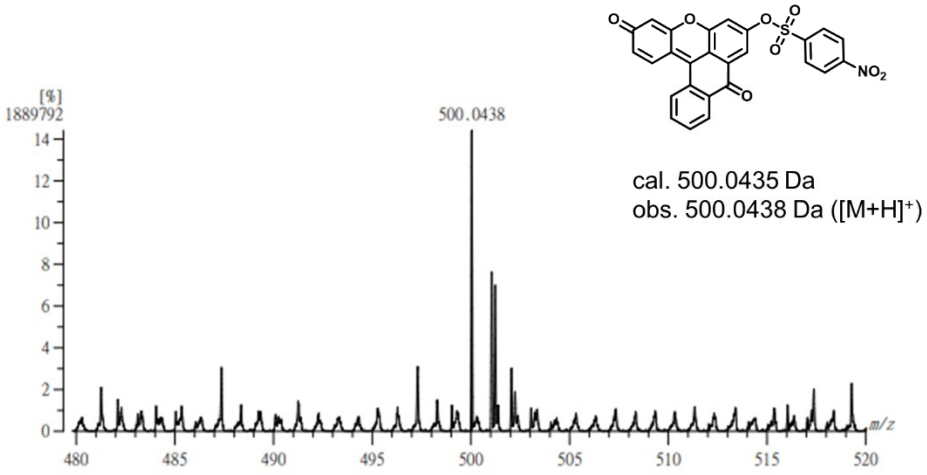

Fig. S8 High-resolution fast atom bombardment (HRFAB) mass spectrum of Sulfonyl-protected **CB** (**2**).

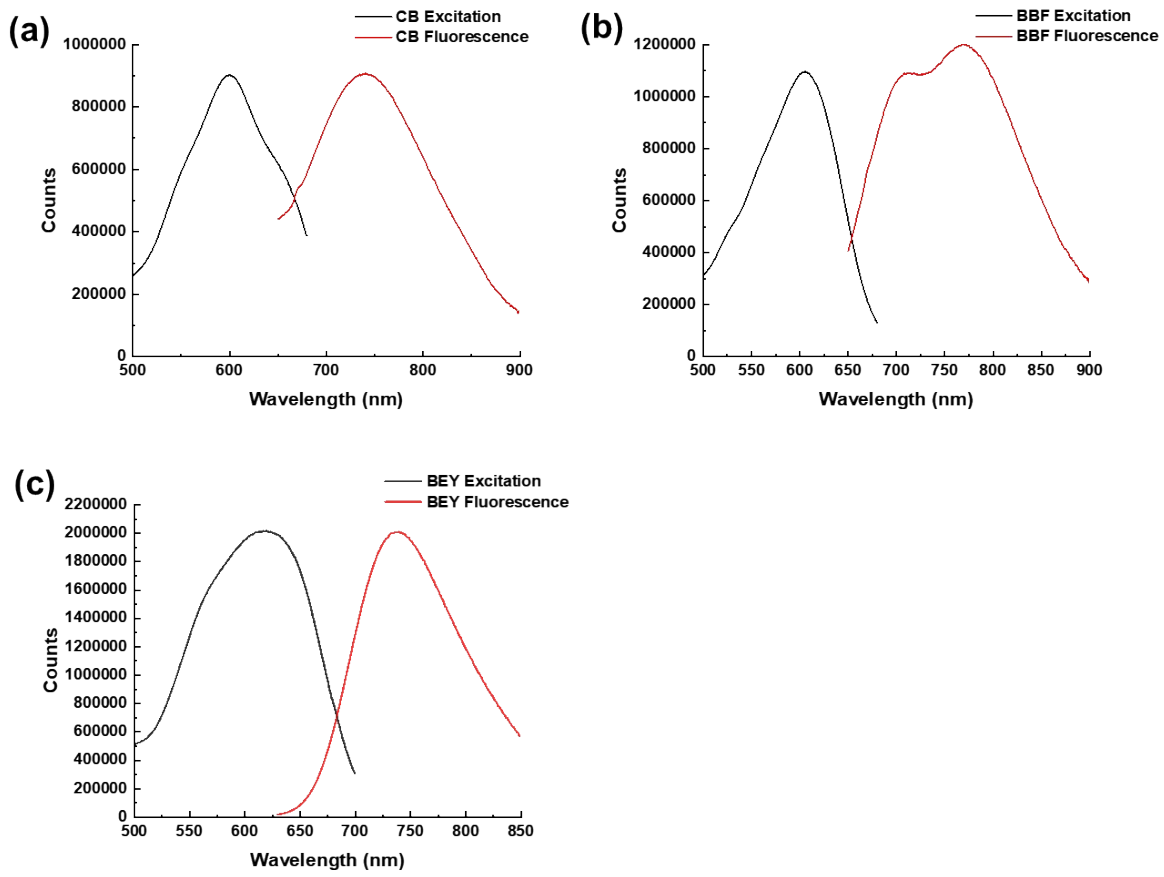

Fig. S9 UV–Vis absorption and fluorescence spectra of (a) **CB** (0.1 mM) (excitation: 600 nm for fluorescence, dwell time: 1.0 s, step: 1.0 nm, excitation and emission bandwidth: 8.0 nm), (b) **BBF** (0.1 mM) (excitation: 605 nm for fluorescence, dwell time: 1.0 s, step: 1.0 nm, excitation and emission bandwidth: 6.0 nm), and (c) **BEY** (0.1 mM) (excitation: 620 nm for fluorescence, dwell time: 1.0 s, step: 1.0 nm, excitation and emission bandwidth: 2.5 nm and 2.0 nm, respectively) dissolved in a mixture of ethanol and DMSO (90:10, v/v) containing 10 mM NaOH.

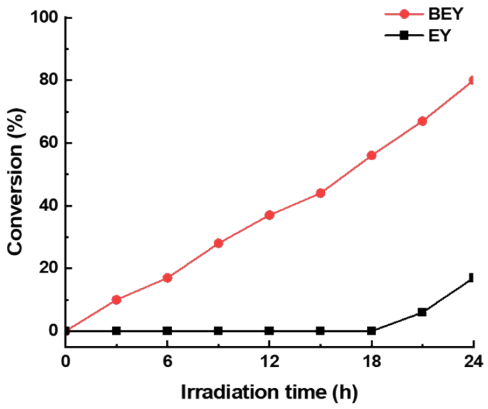

Entry	PC	[OEGMA]:[CTA]:[TEOA]:[PC](mM)	Conv. (%)	Irradiation time (h)	$M_{n,theo}$ (kDa)	$M_{n,exp}$ (kDa)	$Đ$	LED source	Atm.
1	**BEY**	250:1.25:0:0.1	80	5	80	80	1.33	red	air
2	EY	250:1.25:0:0.1	17	5	17	11	1.41	red	air

Fig. S10 Comparison of polymerization kinetics for photo-RAFT photopolymerization under the red-light irradiation.

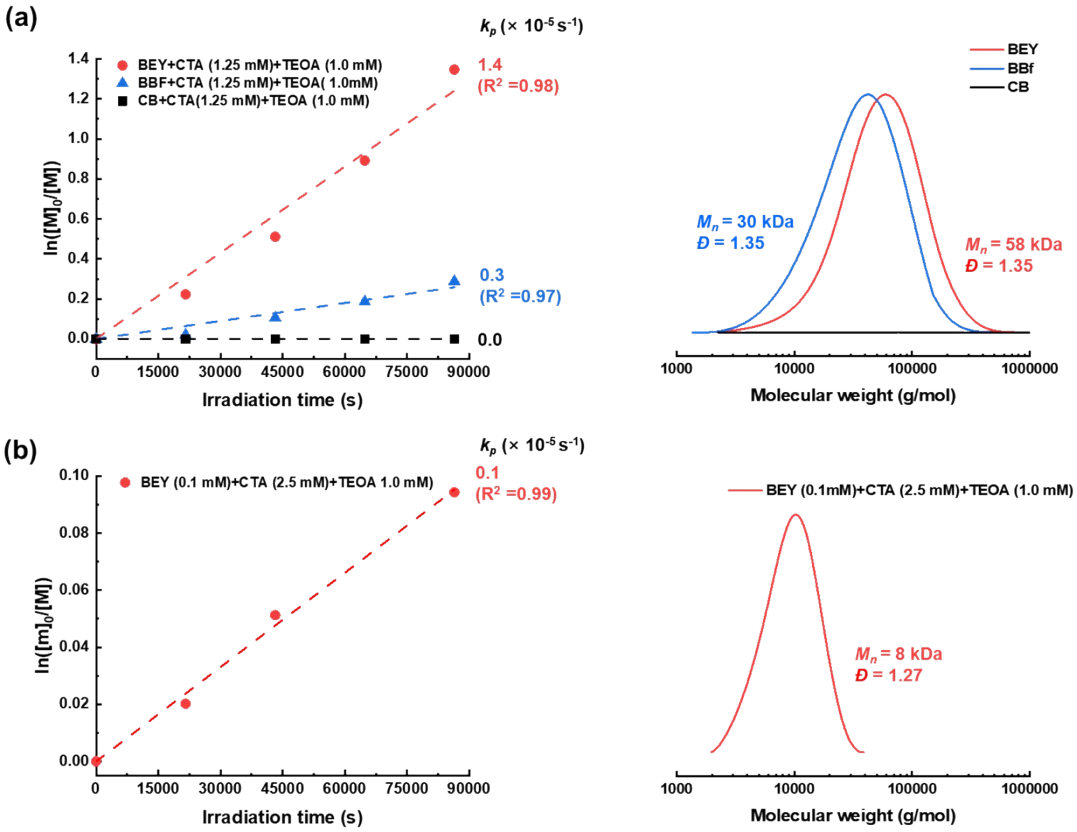

Fig. S11 Polymerization kinetics and GPC traces of (a) BFL (0.1 mM) with CTA (**1**) (1.25 mM) and TEOA (1.0 mM) and (b) **BEY** (0.1 mM) with CTA (**1**) (2.5 mM) and TEOA (1.0 mM) under ambient conditions.

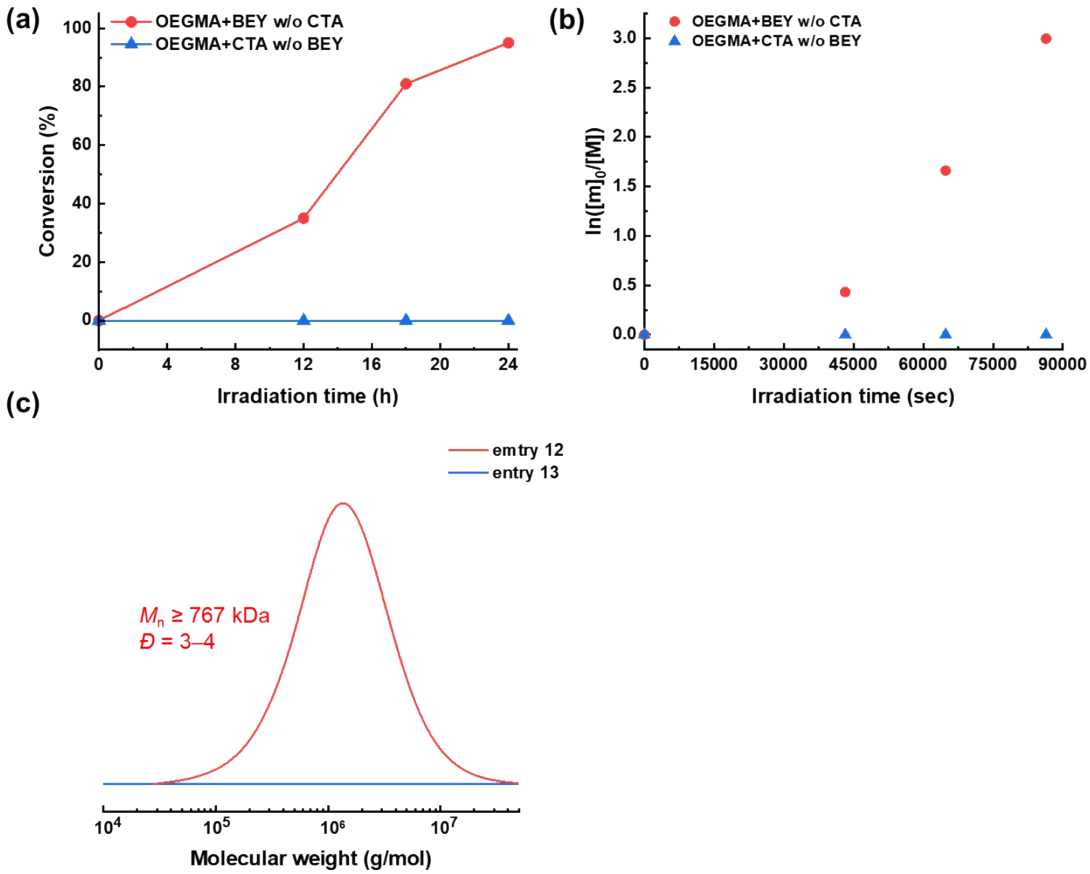

Fig. S12 Raw data corresponding to Table 1 (entries 12 and 13): (a) Monomer conversion using **BEY** (0.1 mM) only and CTA (**1**) (1.25 mM) only, (b) the corresponding first-order kinetic plots, and (c) GPC traces.

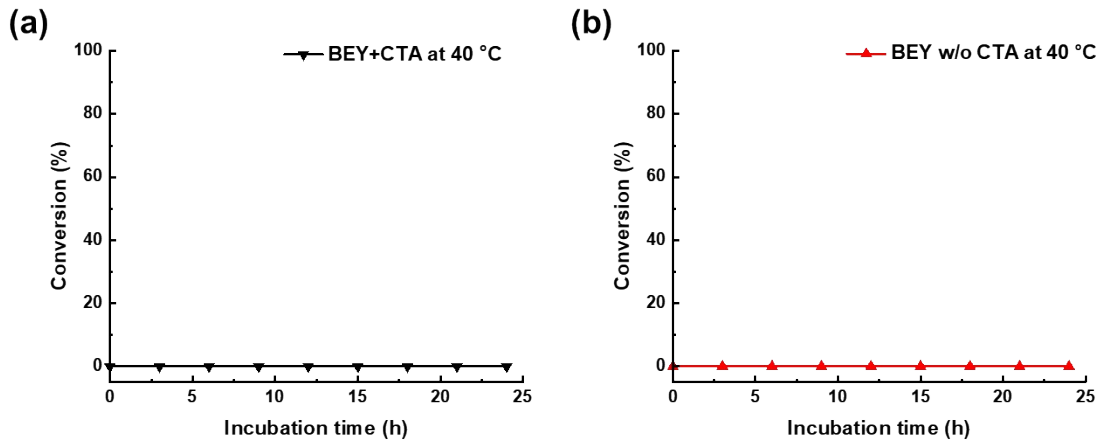

Fig. S13 Negative control experiments at 40 °C under dark conditions for (a) Table 1, entry 3 and (b) Table 1, entry 14.

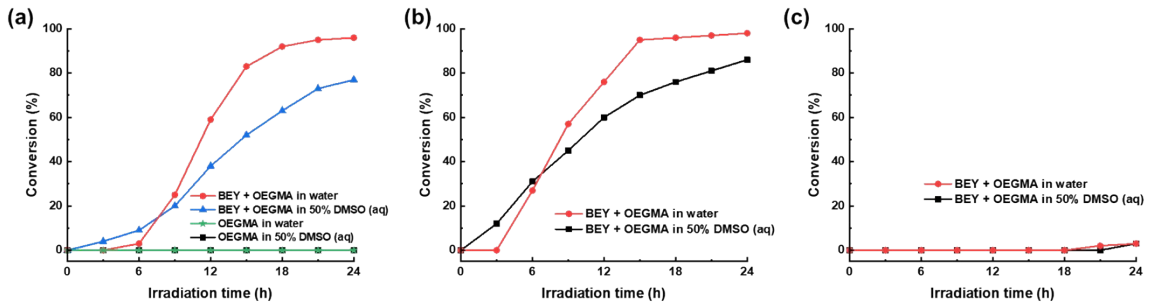

Fig. S14 Photopolymerization of OEGMA (250 mM) using **BEY** (0.1 mM) conducted in pure water or 50% DMSO (aq) under (a) ambient conditions, (b) oxygen-rich conditions, and (c) an argon atmosphere.

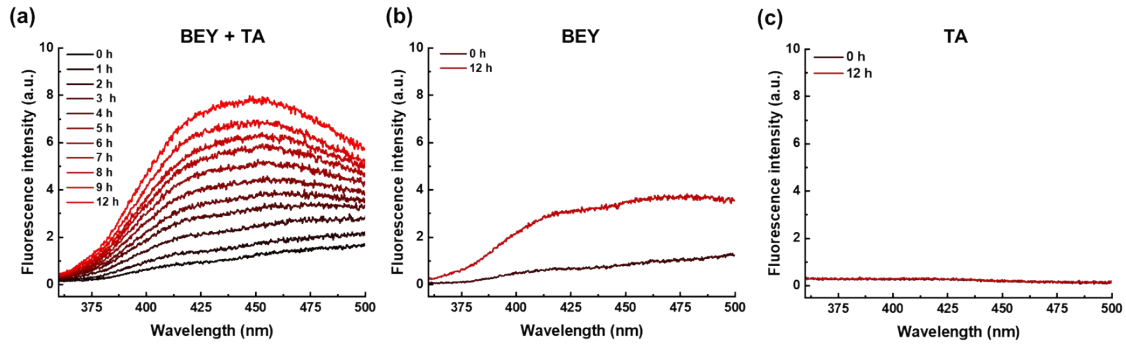

Fig. S15 Detection of the generated hydroxyl radical from **BEY** in water under red-light irradiation.[3] (a) Fluorescence spectra as a function of irradiation time in the presence of **BEY** (0.1 mM) and terephthalic acid (TA) (1 mM), (b) fluorescence spectra of **BEY** only after 12 h of irradiation, and (d) fluorescence spectra of TA only after 12 h of irradiation.

(a)

Entry	[OEGMA]:[**BEY**]:[KO_2]:[H_2O_2] (mM)	Conv.(%)	Reaction time (h)	LED source
1	250:0.1:0:0	77	24	red
2	250:0.1:0:0	0	24	none
3	250:0.1:1:0	93	24	red
4	250:0.1:1:0	0	24	none
5	250:0.1:0:1	95	24	red
6	250:0.1:0:1	0	24	none
7	250:0.1:1:1	93	24	red
8	250:0.1:1:1	0	24	none
9	250:0:1:1	0	24	red

(b)

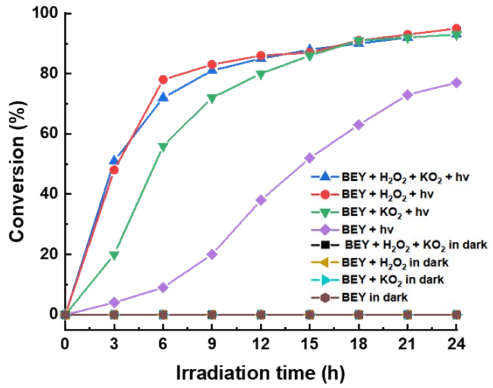

(c)

	Zn	Fe	V	Cr	Ba	Cu	Co	Mn	As	Ag
ppb	65.94	22.59	18.27	17.85	4.11	1.93	1.89	0.51	0.22	0.04

Fig. S16 (a) Summary of the photopolymerization of OEGMA using **BEY** (0.1 mM) in the presence of KO_2 (1 mM) and H_2O_2 (1 mM), (b) polymerization kinetics, and (c) trace metal contaminants analysis determined by inductively coupled plasma mass spectrometry (ICP-MS, NexION 2000, Perkin Elmer).

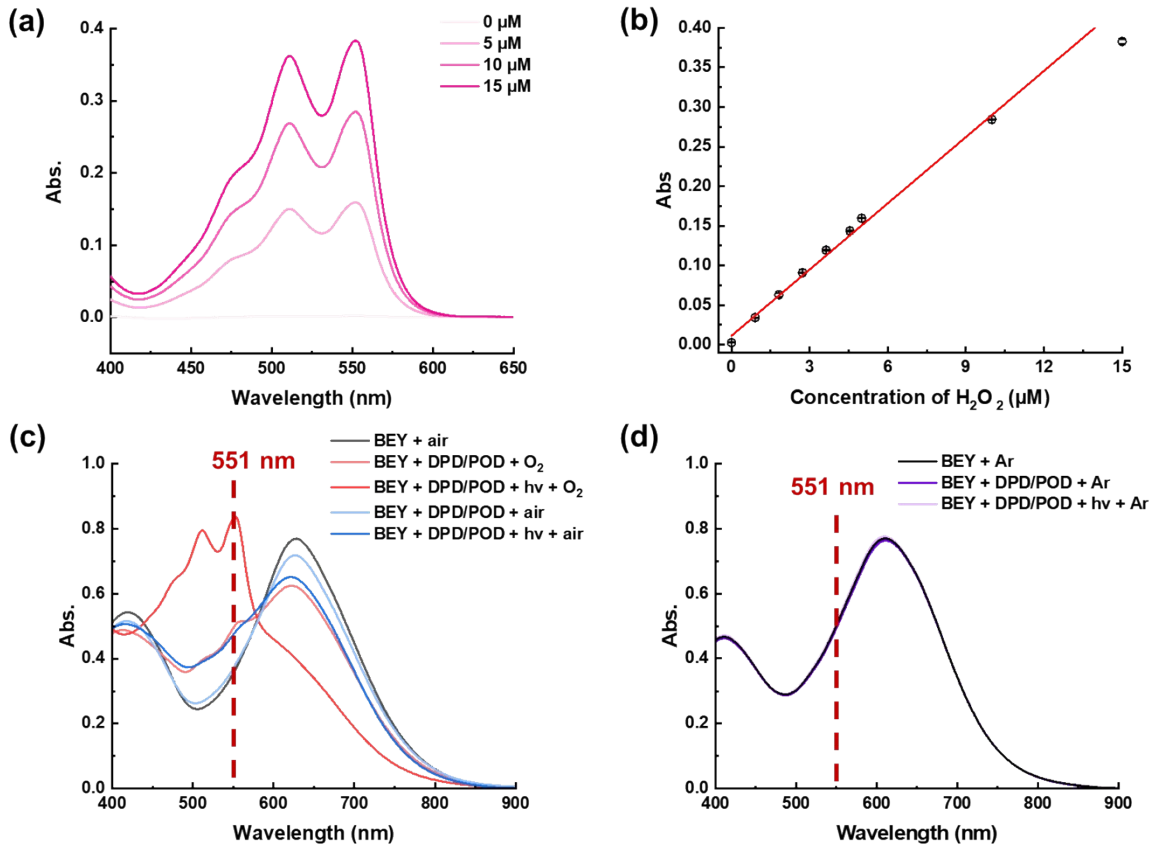

Fig. S17 Raw data from the DPD–POD assay: (a) UV–Vis absorption spectra at varying the concentrations of hydrogen peroxide in the DPD–POD solution; (b) calibration curve; and UV–Vis absorption spectra showing the generation of hydrogen peroxide under (c) aerobic conditions and (d) an argon atmosphere.

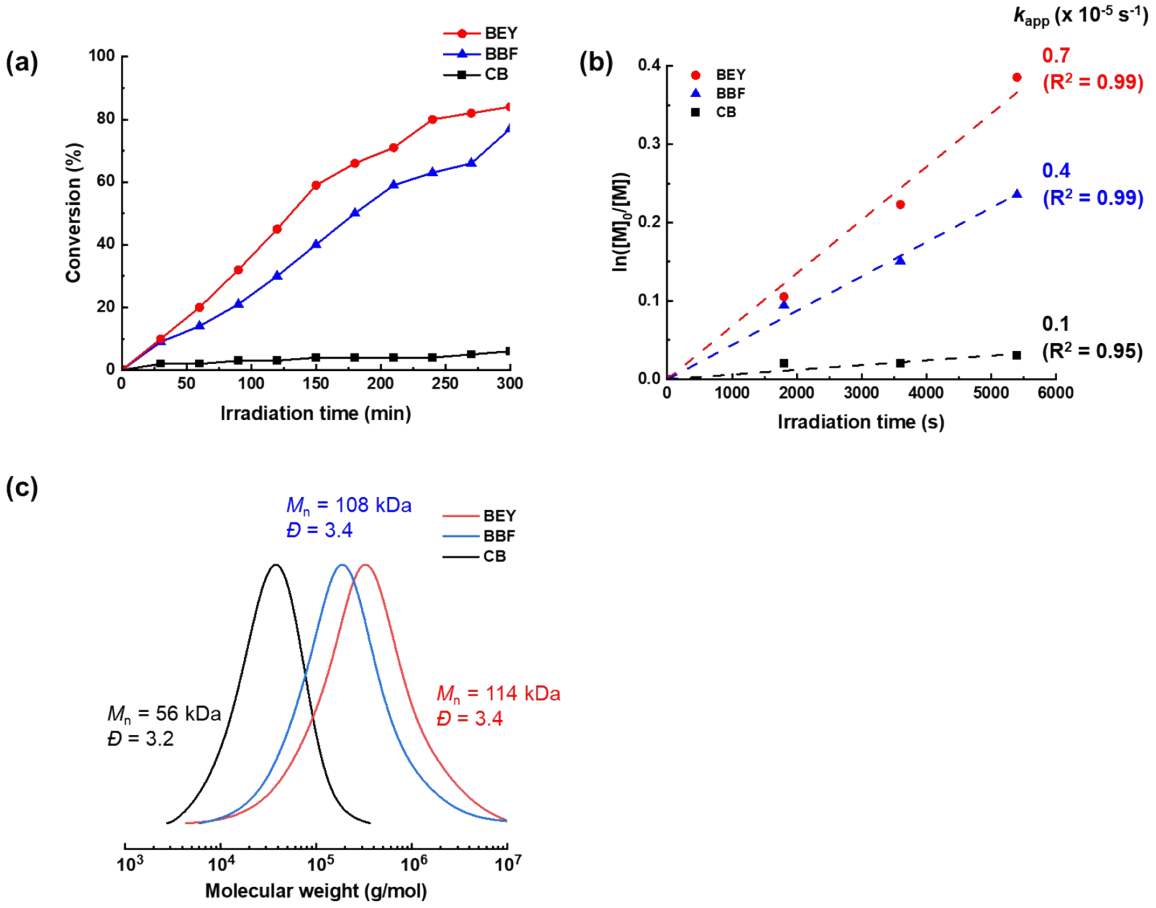

Fig. S18 Raw data corresponding to Table 2 (entries 1–3): (a) monomer conversion, (b) apparent first-order kinetic plots, and (c) GPC traces.

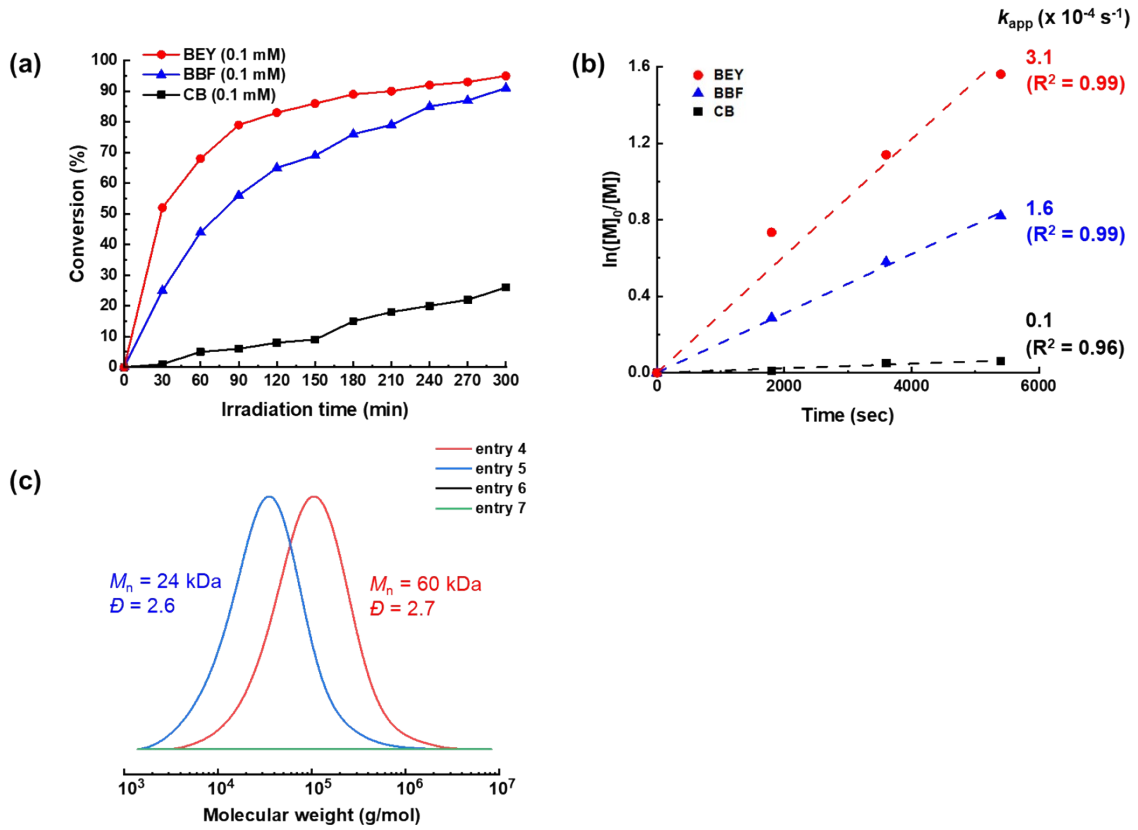

Fig. S19 Raw data corresponding to Table 2 (entries 4–7): (a) monomer conversion, (b) apparent first-order kinetic plots, and (c) GPC traces.

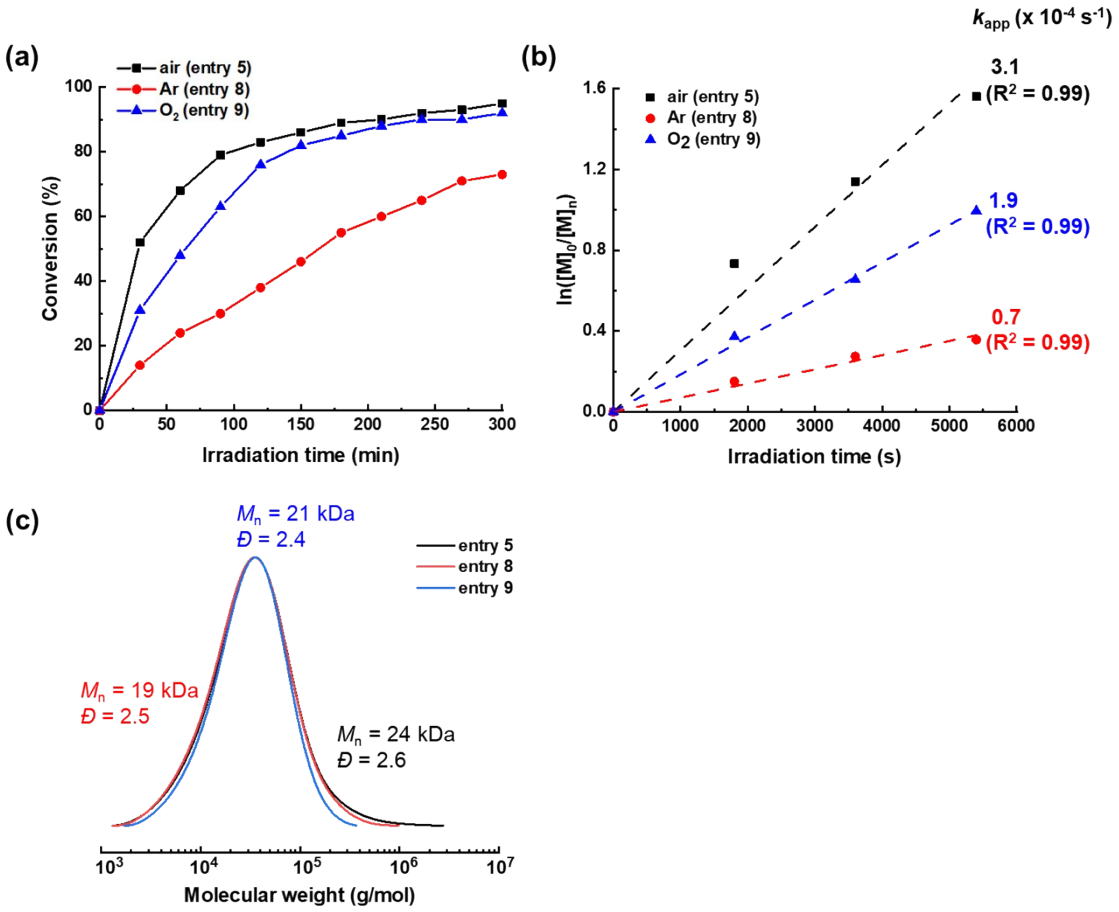

Fig. S20 Raw data corresponding to Table 2 (entries 5, 8 and 9): (a) monomer conversion, (b) apparent first-order kinetic plots, and (c) GPC traces.

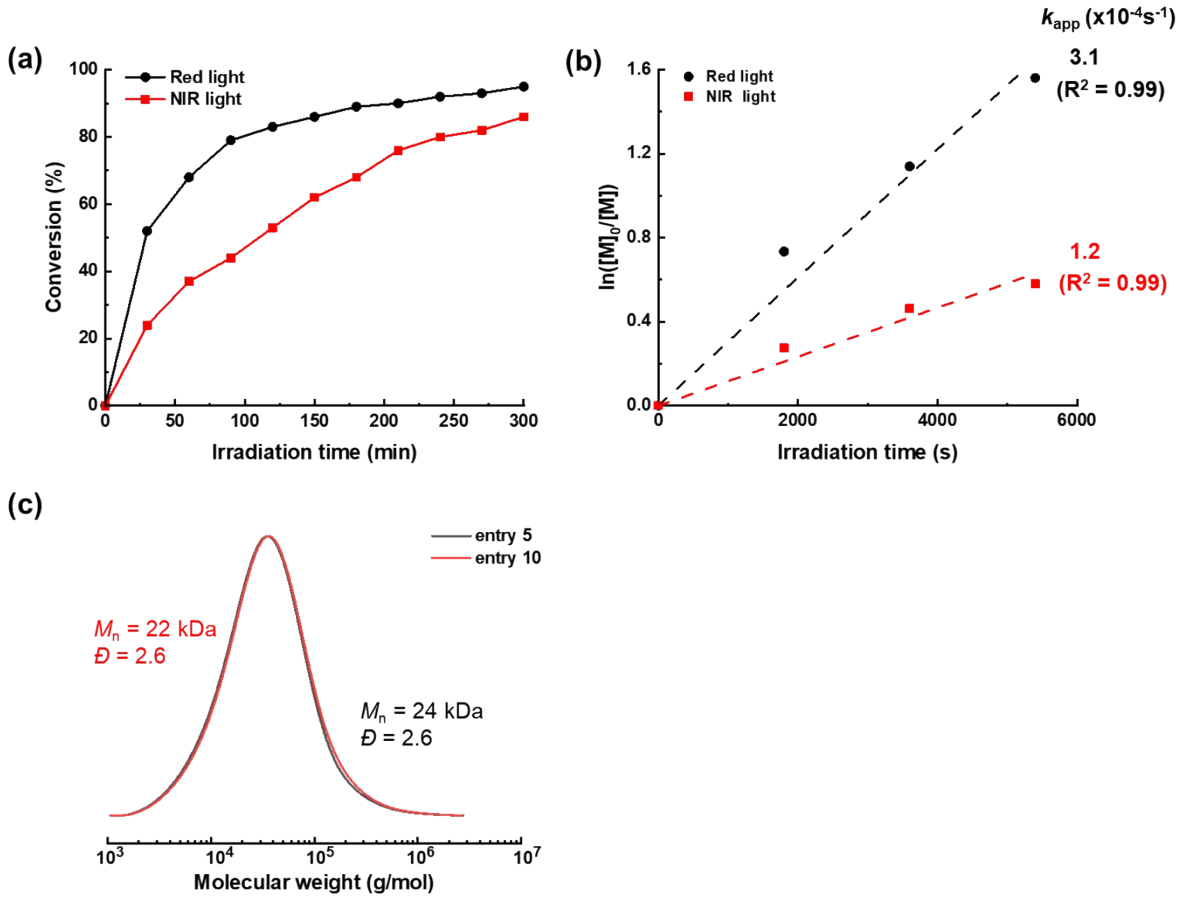

Fig. S21 Raw data corresponding to Table 2 (entries 5 and 10): (a) monomer conversion, (b) apparent first-order kinetic plots, and (c) GPC traces.

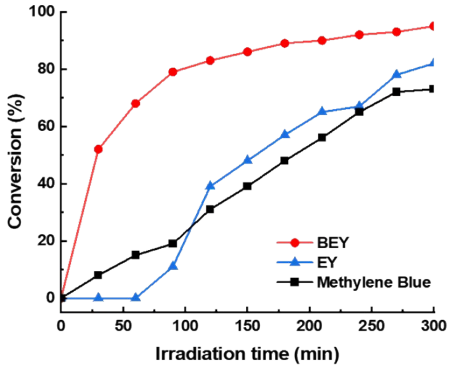

Entry	PC	[OEGMA]:: [TEOA]:[PC](mM)	Conv. (%)	Irradiation time (h)	LED source	Atm.
1	**BEY**	250:100:0.1	95	5	red	air
2	EY	250:100:0.1	82	5	red	air
3	Methylene blue	250:100:0.1	73	5	red	air

Fig. S22 Comparison of polymerization kinetics for free-radical photopolymerization under the red-light irradiation

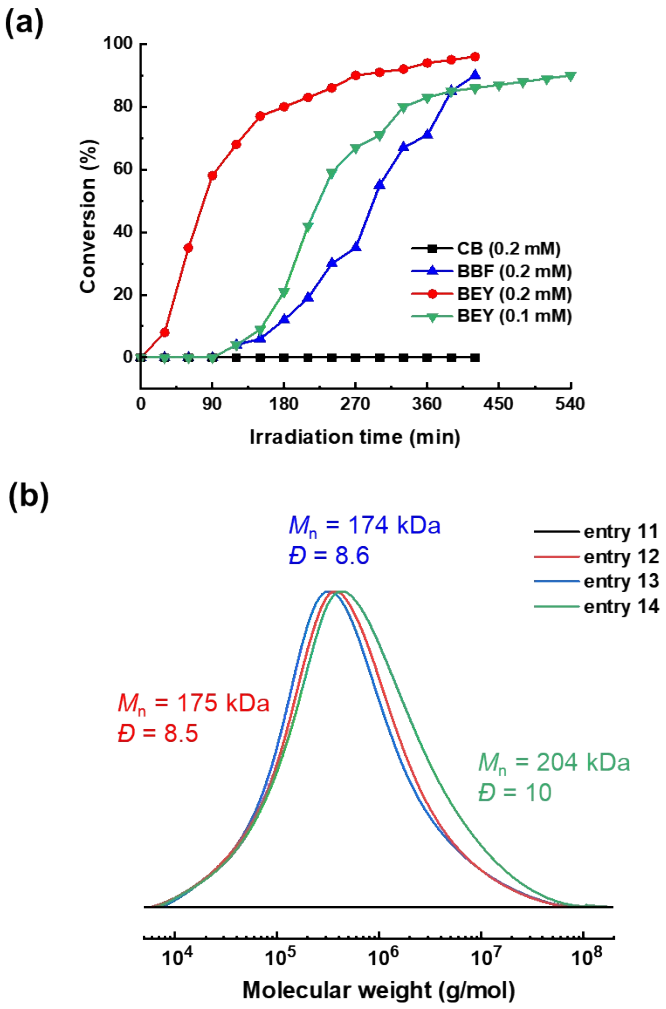

Fig. S23 Raw data corresponding to Table 2 (entries 11–14): (a) monomer conversion and (b) GPC traces.

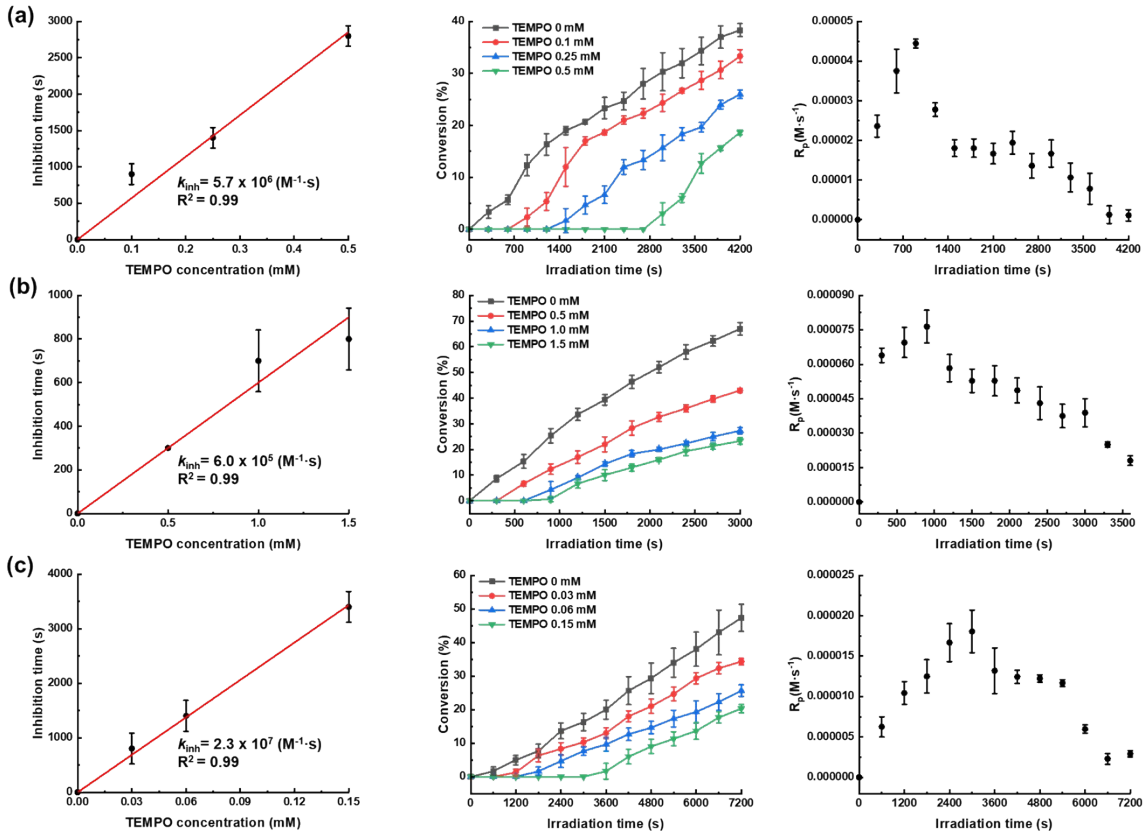

Fig. S24 Experimental results showing the determination of the initiation rate (R_i) and the propagation rate (R_p) under different conditions: (a) **BEY** (0.01 mM) with TEOA (0.1 M), (b) **BEY** (0.1 mM) with TEOA (0.1 M), and (c) **BEY** (0.2 mM) with IOD (0.1 M).

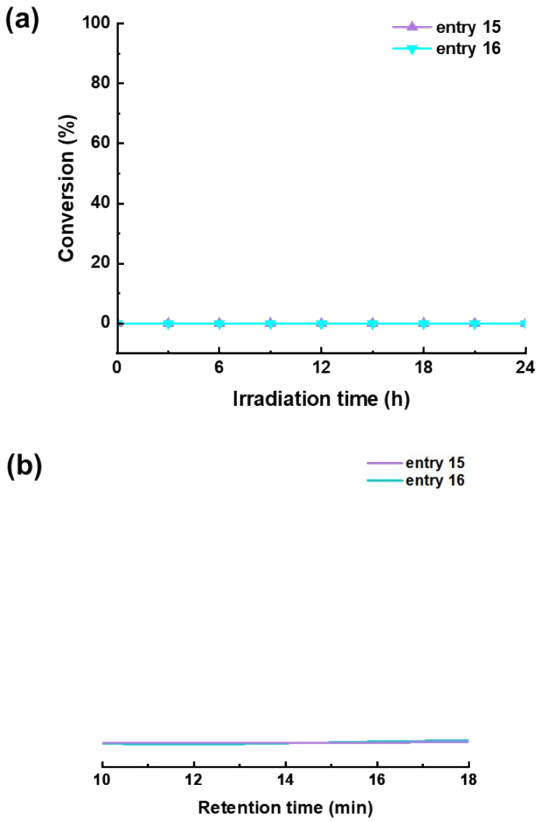

Fig. 25 Raw data corresponding to Table 2 (entries 15 and 16): (a) monomer conversion and (b) GPC traces.

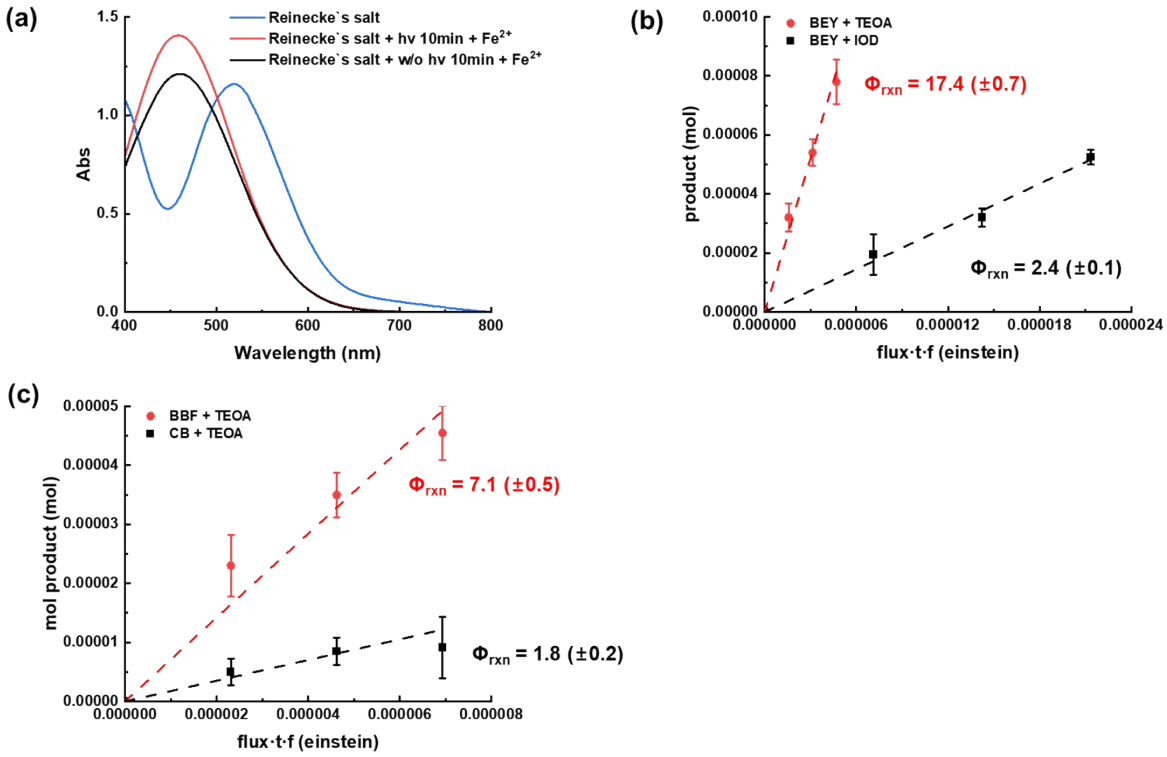

Fig. S26 Experimental results for (a) chemical actinometry using Reinecke's salt and (b, c) determination of reaction quantum yields.

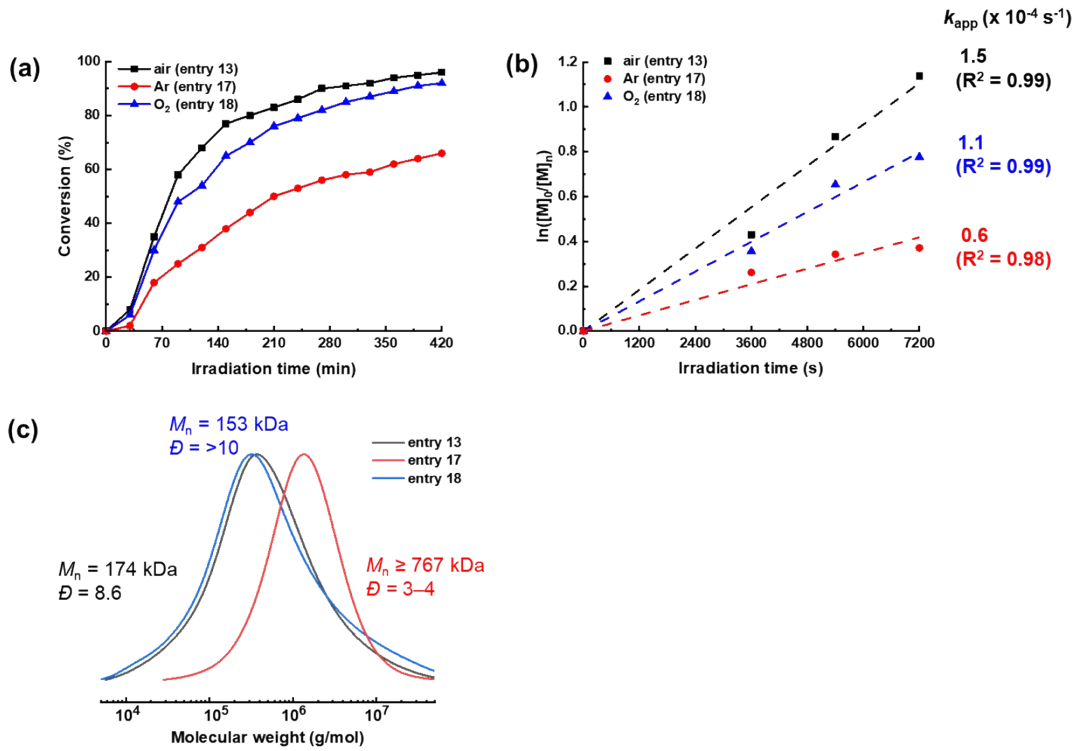

Fig. S27 Raw data corresponding to Table 2 (entries 17 and 18): (a) monomer conversion, (b) apparent first-order kinetic plots, and (c) GPC traces.

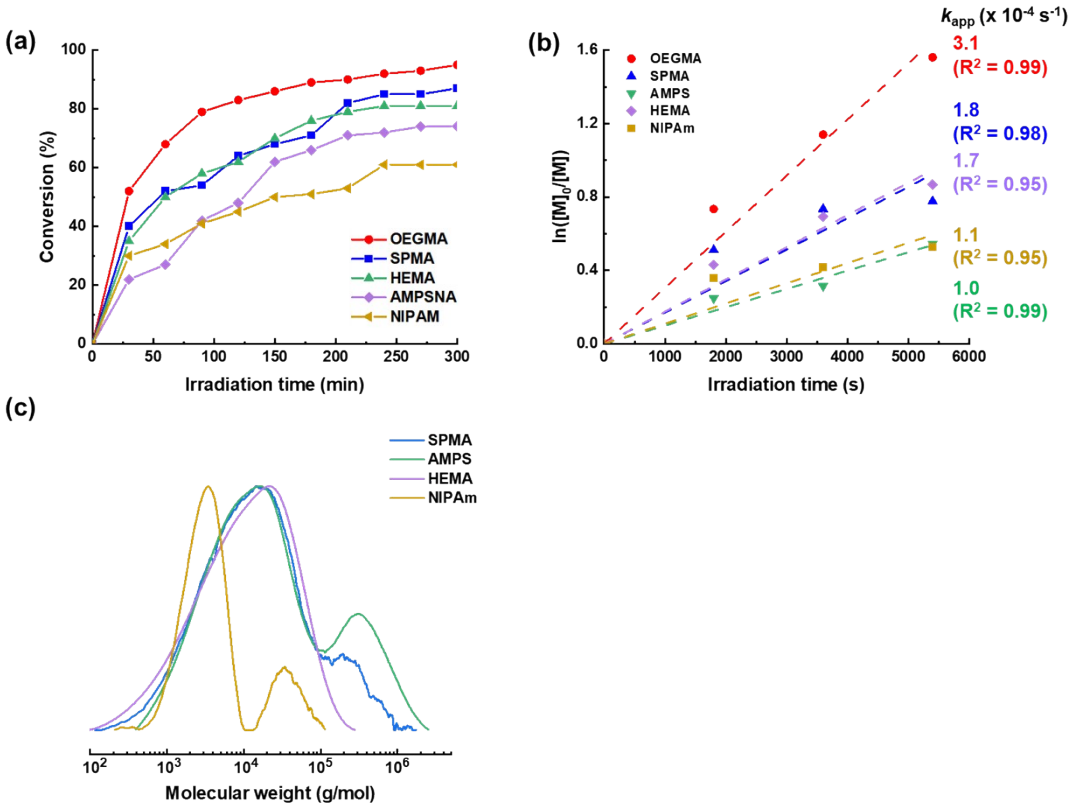

Fig. S28 Raw data corresponding to Table 4: (a) monomer conversion, (b) apparent first-order kinetic plots, and (c) GPC traces.

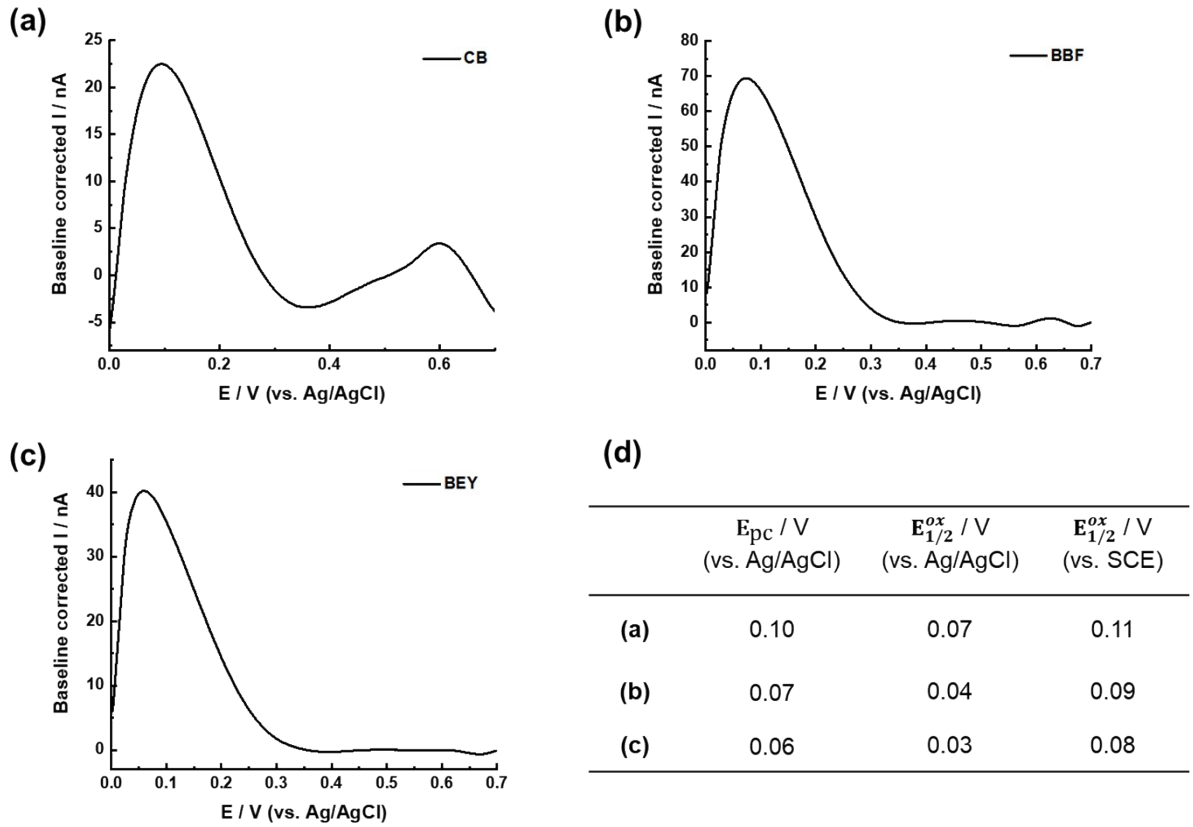

(d)

	E_{pc} / V (vs. Ag/AgCl)	$E^{ox}_{1/2}$ / V (vs. Ag/AgCl)	$E^{ox}_{1/2}$ / V (vs. SCE)
(a)	0.10	0.07	0.11
(b)	0.07	0.04	0.09
(c)	0.06	0.03	0.08

Fig. S29 LSV measurement for the oxidation potential of (a) **CB**, (b) **BBF**, and (C) **BEY**. (d) A summary of the measured oxidation potential values at a scan rate of 0.1 V/s. Each BFL was measured at a concentration of 1.0 mM in 50% DMSO (aq) containing 10 μM NaOH.

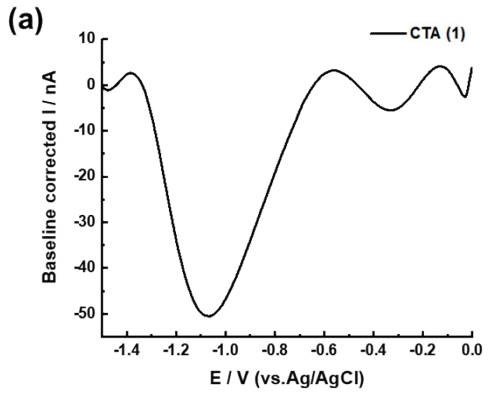

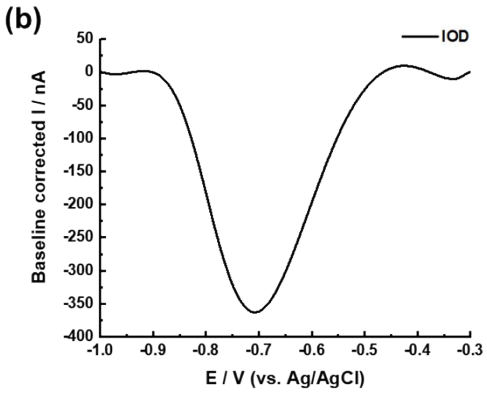

(c)

	E_{pc} / V (vs. Ag/AgCl)	$E_{1/2}^{red}$ / V (vs. Ag/AgCl)	$E_{1/2}^{red}$ / V (vs. SCE)
(a)	-1.07	-1.04	-1.08
(b)	-0.71	-0.68	-0.73

Fig. S30 LSV measurement for the reduction potential of (a) CTA (**1**) and (b) IOD. (c) A summary of the measured oxidation potential values at a scan rate of 0.1 V/s. Each compound was measured at a concentration of 1.0 mM in ethanolic solution containing 10 μM NaOH.

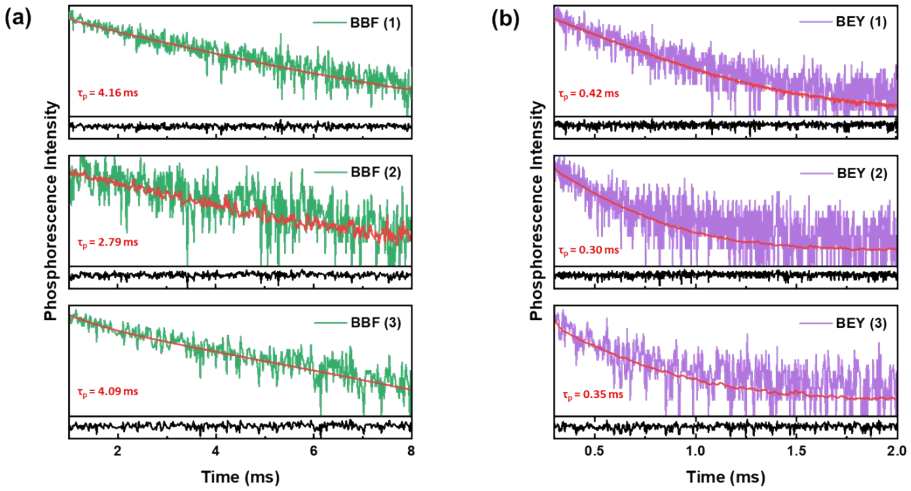

Fig. S31 Phosphorescence decay profiles of (a) **BBF** and (b) **BEY** with 600 nm excitation. Red lines are the best-fit curves, and lower black lines show the IRF.

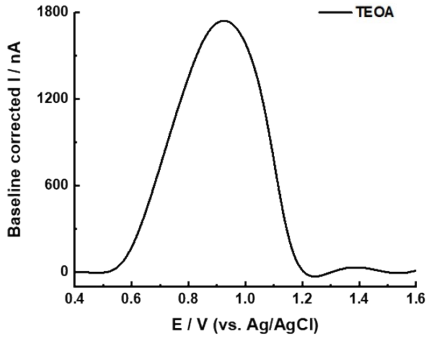

	E_{pc} / V (vs. Ag/AgCl)	$E_{1/2}^{ox}$ / V (vs. Ag/AgCl)	$E_{1/2}^{ox}$ / V (vs. SCE)
(a)	0.93	0.90	0.95

Fig. S32 LSV measurement for the oxidation potential of TEOA (1.0 mM) in 50% DMSO (aq) containing 10 μM NaOH and a summary of the measured oxidation potential values at a scan rate of 0.1 V/s.

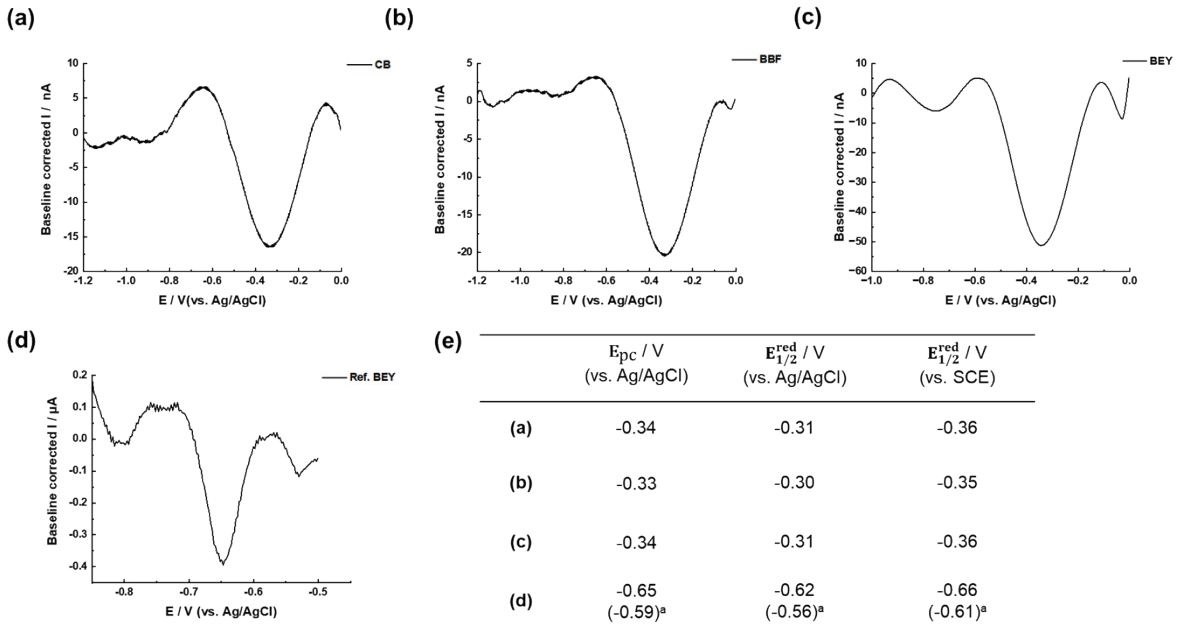

(e)

	E_{pc} / V (vs. Ag/AgCl)	$E^{red}_{1/2}$ / V (vs. Ag/AgCl)	$E^{red}_{1/2}$ / V (vs. SCE)
(a)	-0.34	-0.31	-0.36
(b)	-0.33	-0.30	-0.35
(c)	-0.34	-0.31	-0.36
(d)	-0.65 (-0.59)[a]	-0.62 (-0.56)[a]	-0.66 (-0.61)[a]

Fig. S33 LSV measurements for the reduction potential of (a) **CB**, (b) **BBF**, (C) **BEY**, and (d) **BEY** under literature conditions. (e) A summary of the measured reduction potential values at a scan rate of 0.1 V/s. Each BFL was measured at a concentration of 1 mM in 50% DMSO (aq) containing 10 µM NaOH. [a]Reported values under CH_2Cl_2 with 0.1 M tetrabutylammonium perchlorate as the supporting electrolyte from the literature.[4]

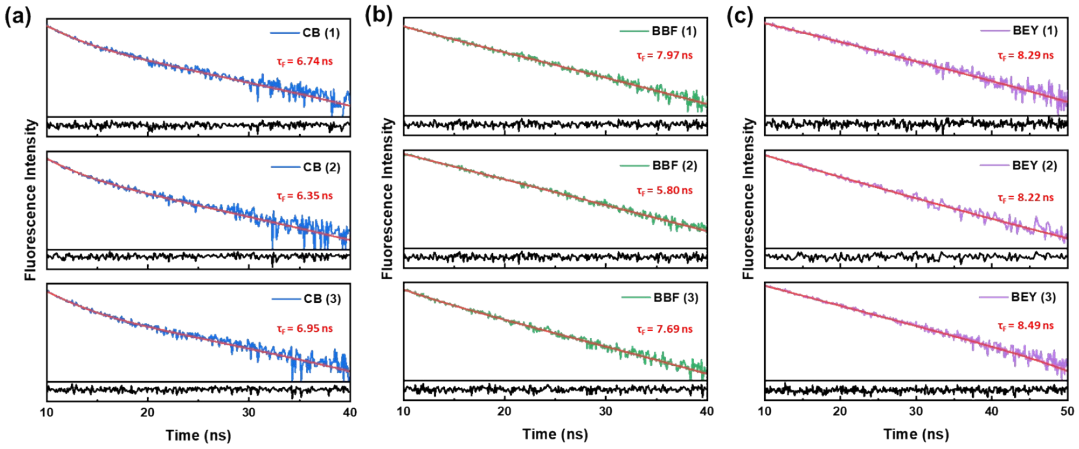

Fig. S34 Fluoresce decay profiles of (a) **CB**, (b) **BBF**, and (c) **BEY** with 600 nm excitation. Red lines are the best-fit curves, and lower black lines denote IRF.

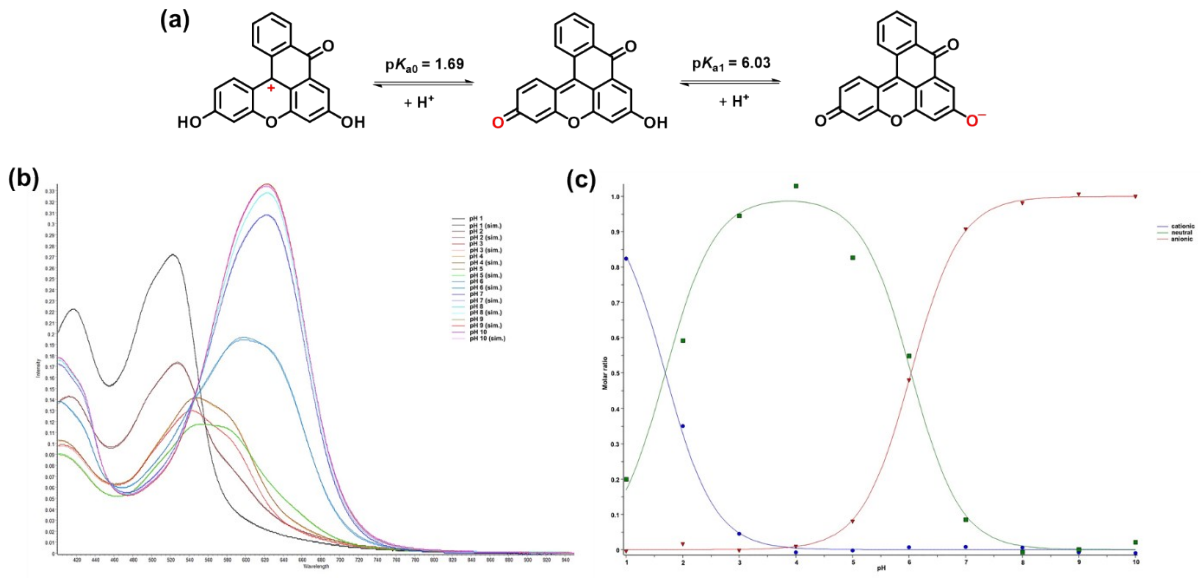

Fig. S35 Protolytic equilibria of **CB**: (a) suggested structures with dissociation constants in 10% DMSO in pH buffer solution (aq), (b) UV–Vis absorption spectra under varying pH conditions, and (c) relative concentrations of each protolytic species as a function of pH value, simulated by DATAN software.

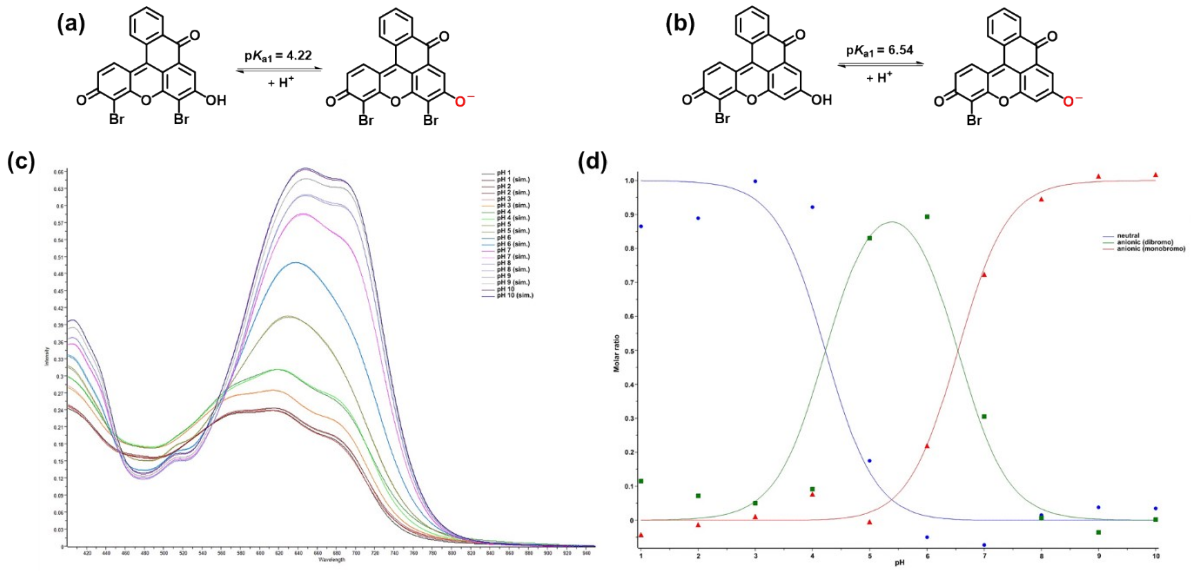

Fig. S36 Protolytic equilibria of **BBF**: (a-b) suggested structures with dissociation constants of bridged dibromo- and bridged monobromo-fluorescein in 10% DMSO in pH buffer solution (aq), (c) UV–Vis absorption spectra under varying pH conditions, and (d) relative concentrations of each protolytic species as a function of pH value, simulated by DATAN software.

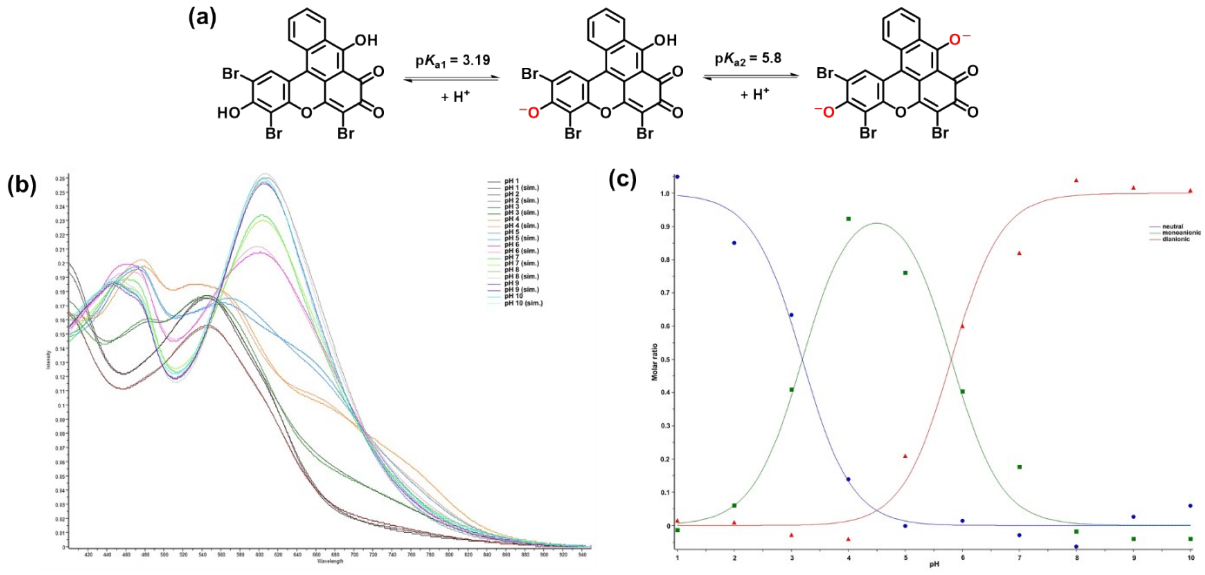

Fig. S37 Protolytic equilibria of **BEY**: (a) suggested structures with dissociation constants in 10% DMSO in pH buffer solution (aq), (b) UV–Vis absorption spectra under varying pH conditions, and (c) relative concentration of each protolytic species as a function of pH value, simulated by DATAN software.

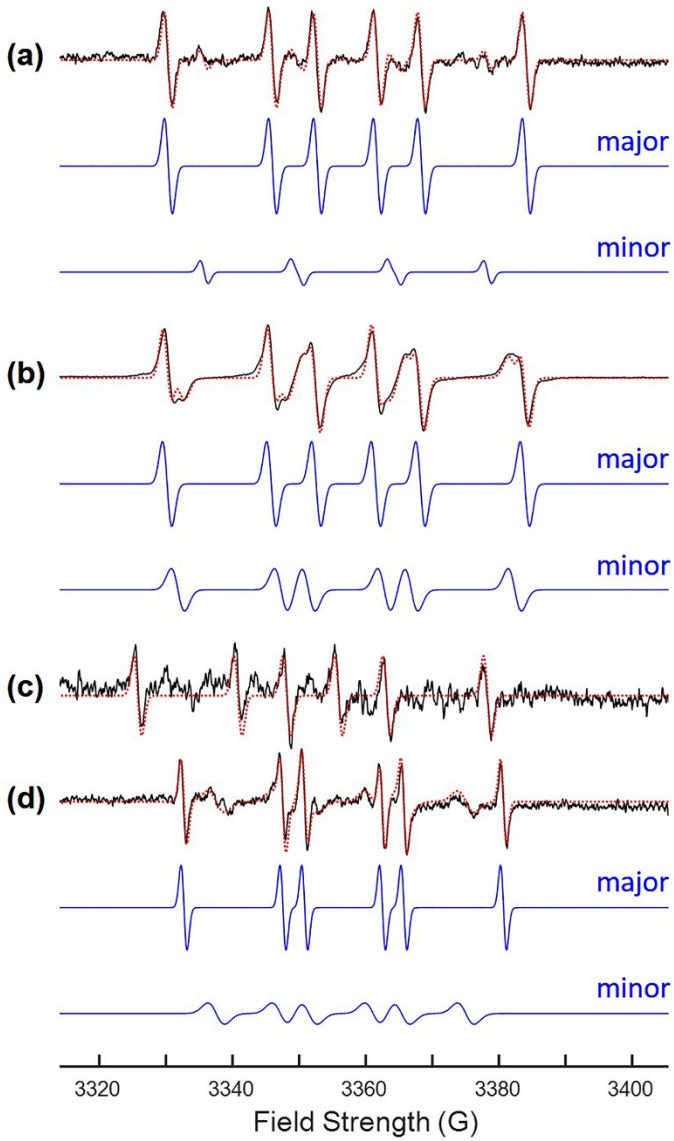

Fig. S38 Detailed EPR spectra obtained from 50% DMSO (aq) of (a) **BEY** + DMPO, (b) **BEY** + DMPO + TEOA, (c) **BEY** + DMPO + IOD, (d) **BEY** + DMPO+ CTA, and (e) DMPO after 20 min of red-light irradiation in 50% DMSO (aq). The corresponding simulations are shown as blue lines below the experimental spectra and are overlaid on the spectra as red dots.

(a)

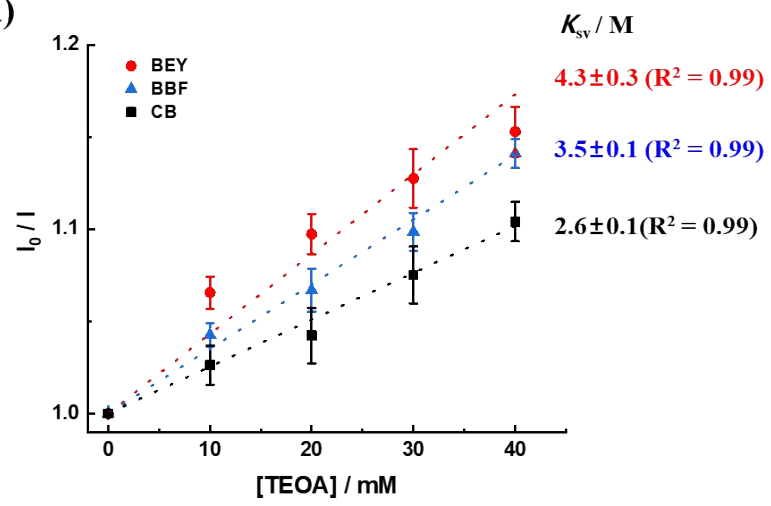

(b)

	K_{sv} (M^{-1})	τ_0 (ns)	k_q ($M^{-1}\cdot s^{-1}$)
CB	2.6±0.1	6.7±0.3	3.9±0.2 × 10^8
BBF	3.5±0.1	7.2±1.2	4.9±0.8 × 10^8
BEY	4.3±0.4	8.3±0.1	5.2±0.5 × 10^8

Fig. S39 (a) Stern-Volmer analysis of BFLs with TEOA and (b) summary of the quantitative results.

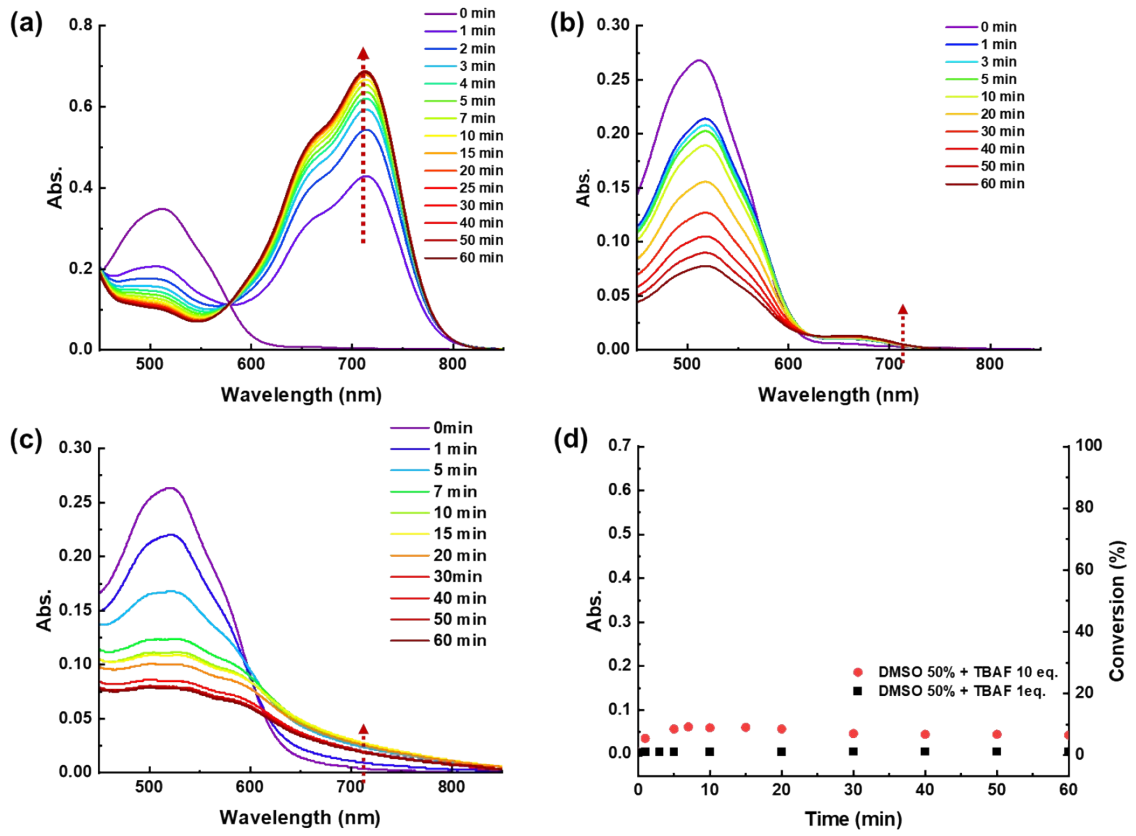

Fig. S40 Kinetic study of the reaction between compound (**2**) and fluoride ions under different conditions. UV–Vis absorption spectra of (**2**) (50 μM) with (a) fluoride ions (1 equiv.) at 37 °C, (b) fluoride ions (1 equiv.) at 25 °C, and (c) fluoride ions (10 equiv.) at 25 °C. (d) Summary of the results from (b) and (c).

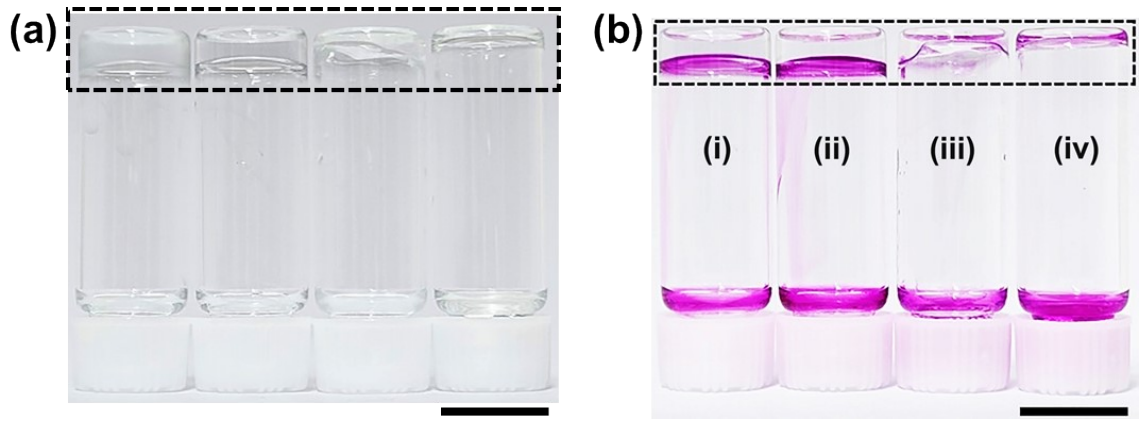

Fig. S41 Hydrogelation control study. Positive control demonstrating hydrogel formation using PEGDA (0.6 M) and TEOA (0.75 M) in 20% DMSO (aq) at varying concentration of **CB**. The images show the samples (a) before and (b) after staining using phenolphthalein/NaOH to visualize hydrogel: (i) 15 μM after 8 min of irradiation, (ii) 10 μM after 14 min of irradiation, (iii) 7.5 μM of 15 min irradiation, and (iv) 5 μM after 1 h of irradiation. The scale bars indicate 1.5 cm.

(a)

Entry	Conc. TBAF (equiv.)	[OEGMA]: [TEOA]: [**CB** (**2**)] (mM)	Conv. (%)	Irradiation time (h)
1	0.2 mM (1.0)	250:200:0.2	82	6
2	0.1 mM (0.5)	250:200:0.2	34	6
3	0.05 mM (0.25)	250:200:0.2	8	6
4	0.02 mM (0.1)	250:200:0.2	0	6
5	0	250:200:0.2	0	6

(b)

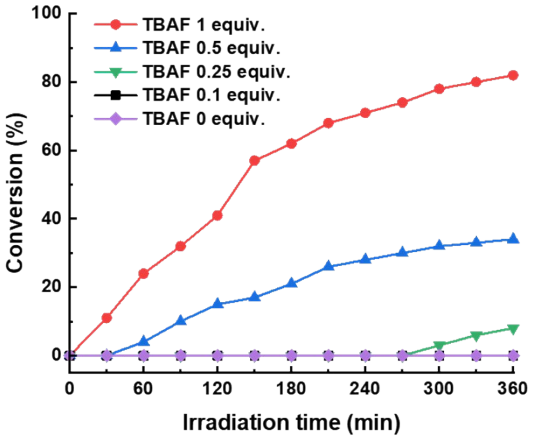

Fig. S42 (a) Summary of the photopolymerization of OEGMA in the presence of **CB** (**2**) and TEOA with varying concentrations of TBAF and (b) monomer conversion as a function of irradiation time.

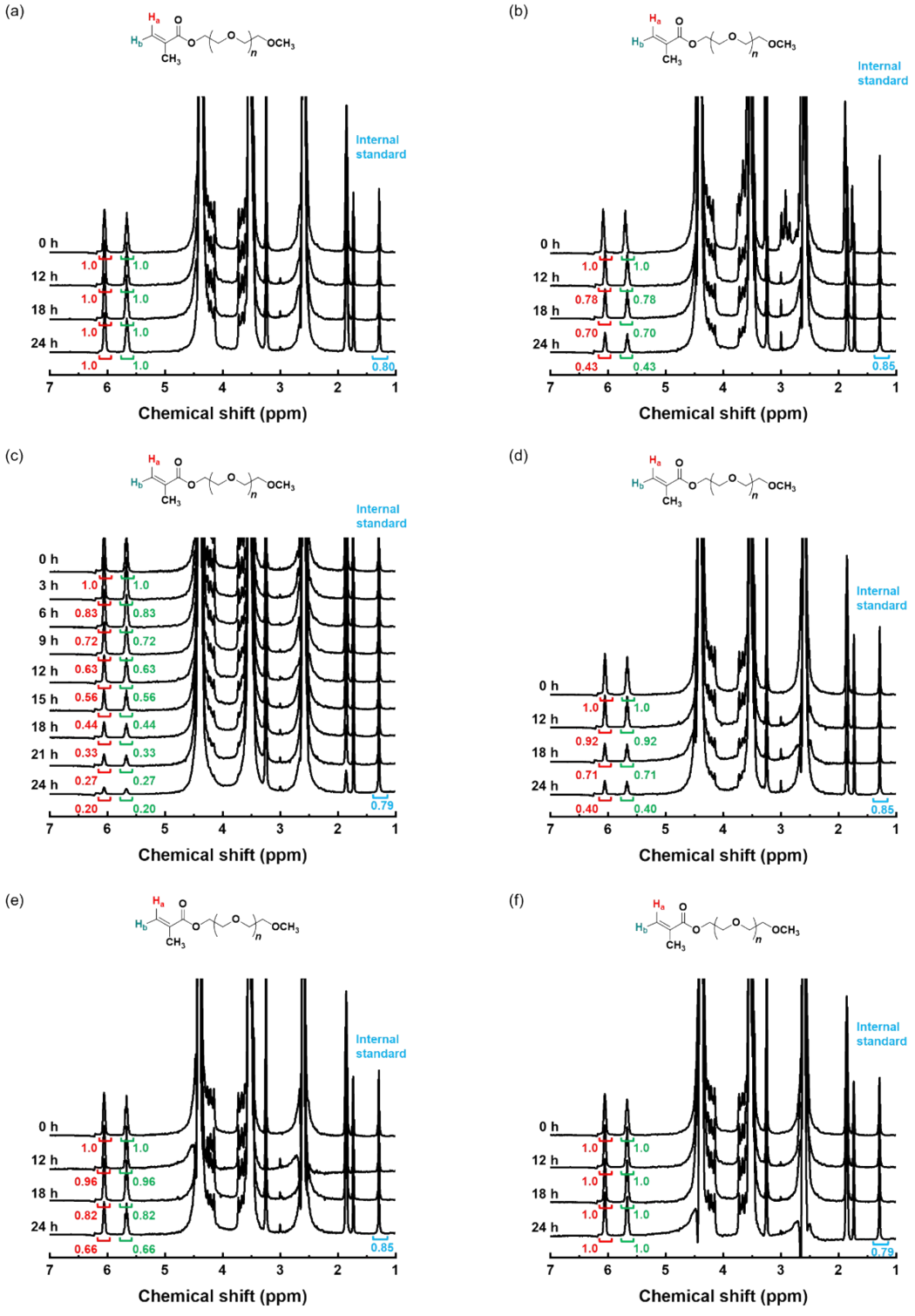

Fig. S43 ^{1}H NMR monitoring of OEGMA conversion, showing redrawn representations of the raw data from Table 1: (a) entry 1, (b) entry 2, (c) entry 3, (d) entry 4, (e) entry 5, and (f) entry 6.

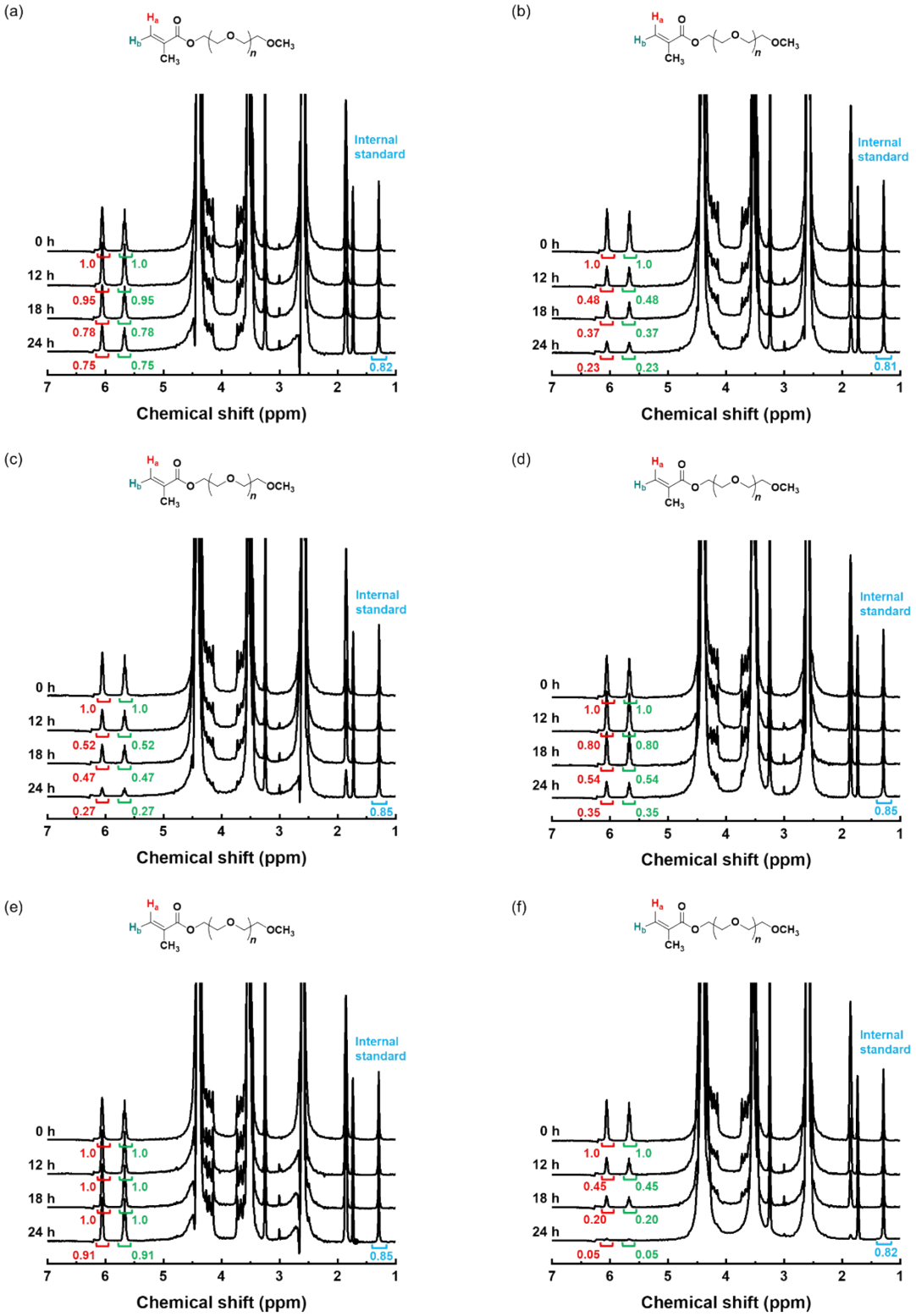

Fig S44 ^{1}H NMR monitoring of OEGMA conversion, showing redrawn representation of the raw data from Table 1: (a) entry 7, (b) entry 8, (c) entry 9, (d) entry 10, (e) entry 11, and (f) entry 12.

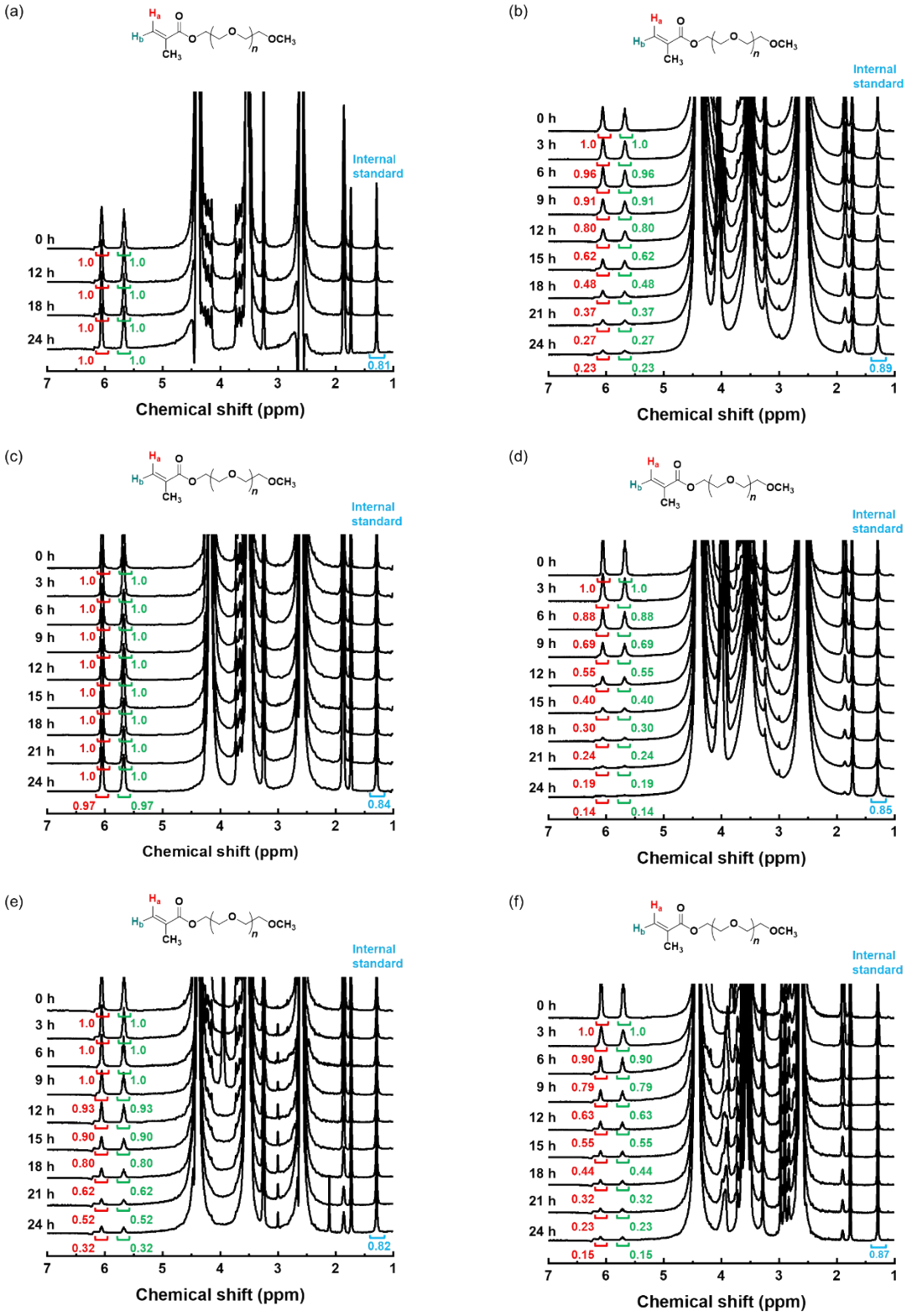

Fig. S45 ^{1}H NMR monitoring of OEGMA conversion, showing redrawn representations of the raw data from Table 1: (a) entry 13, (b) entry 14, (c) entry 15, (d) entry 16, (e) entry 17, and (f) entry 18.

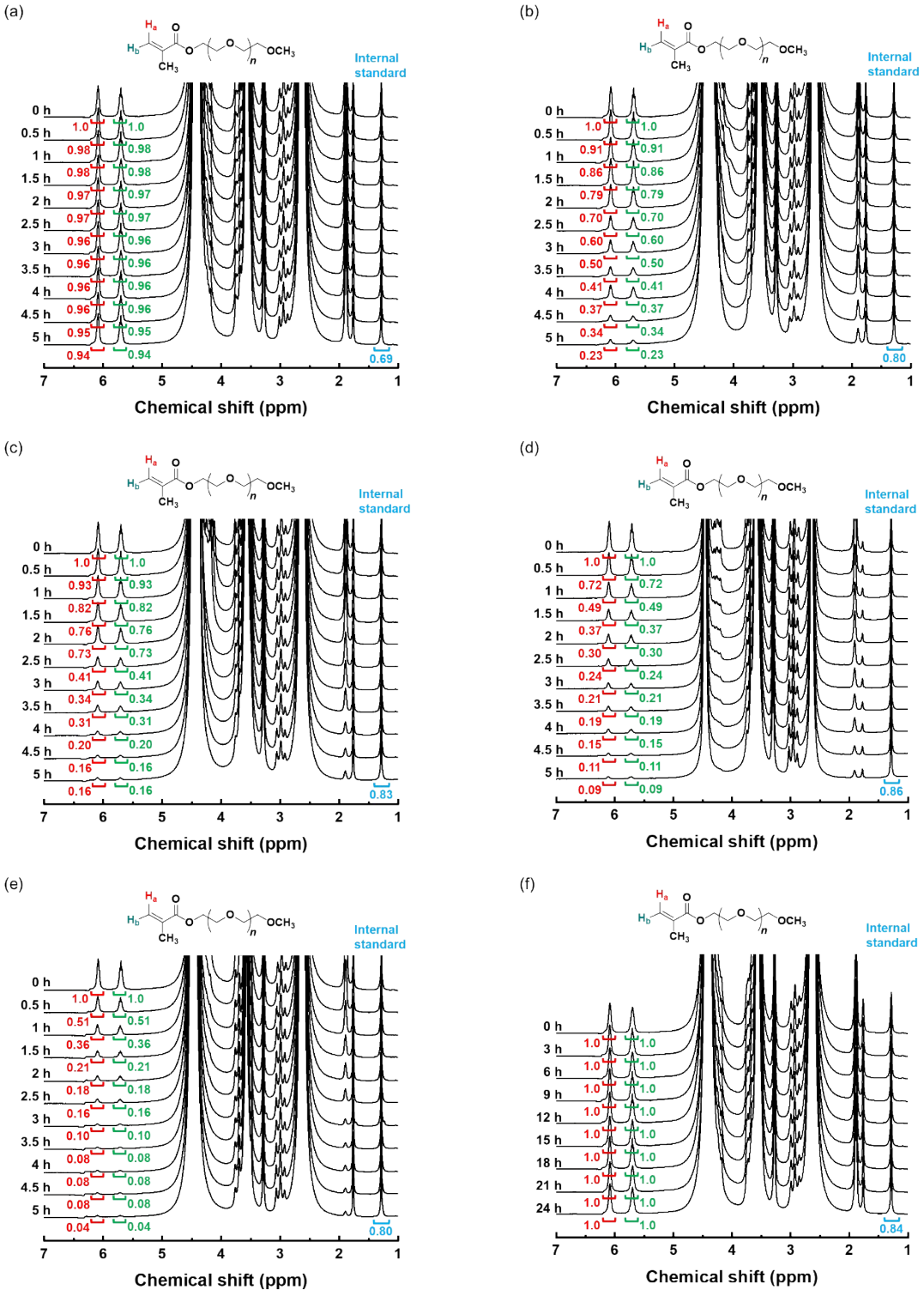

Fig. S46 ^{1}H NMR monitoring of OEGMA conversion, showing redrawn representations of the raw data from Table 2: (a) entry 1, (b) entry 2, (c) entry 3, (d) entry 4, (e) entry 5, and (f) entry 6.

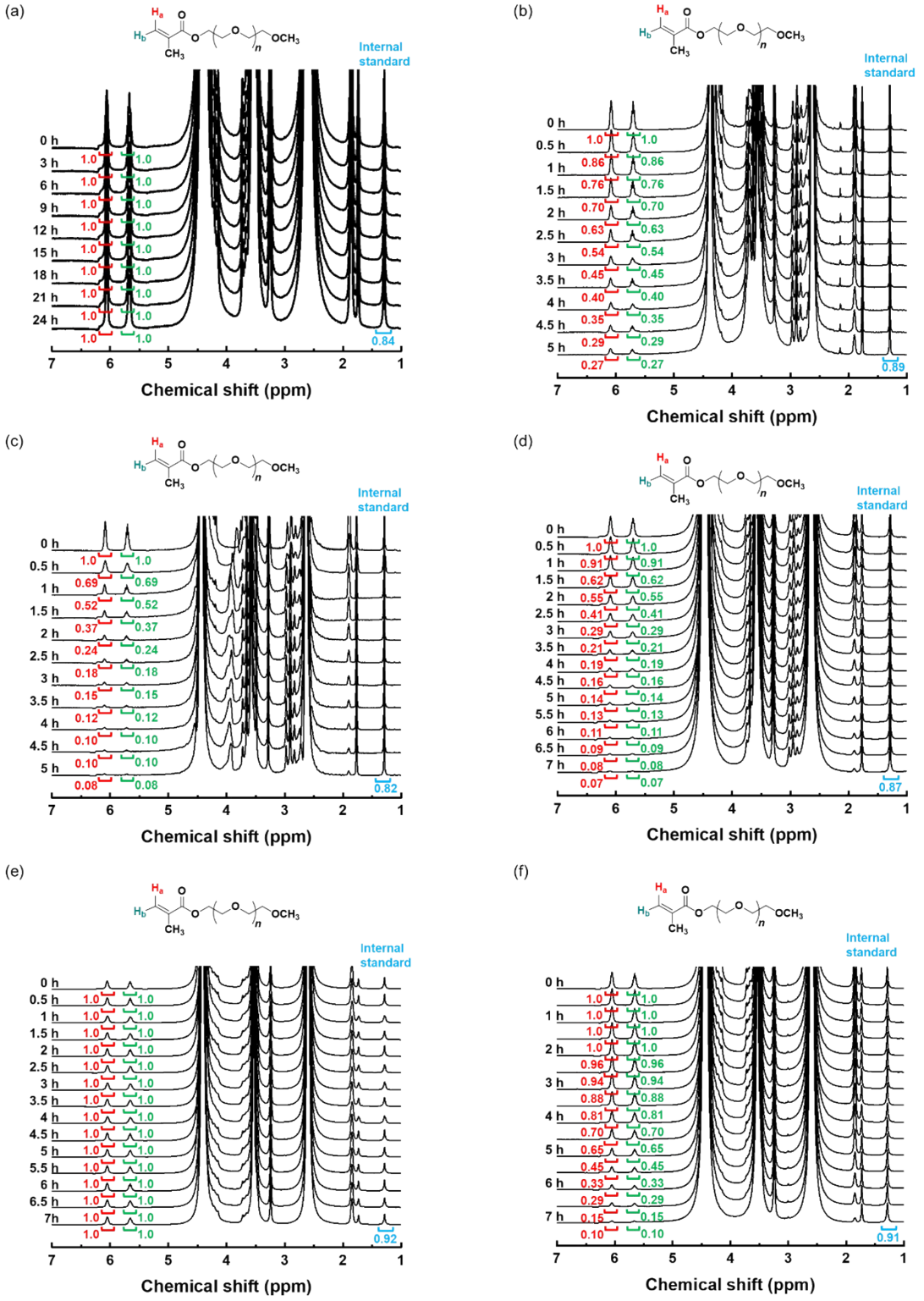

Fig. S47 ^{1}H NMR monitoring of OEGMA conversion, showing representations of the raw data from Table 2: (a) entry 7, (b) entry 8, (c) entry 9, (d) entry 10, (e) entry 11, and (f) entry 12.

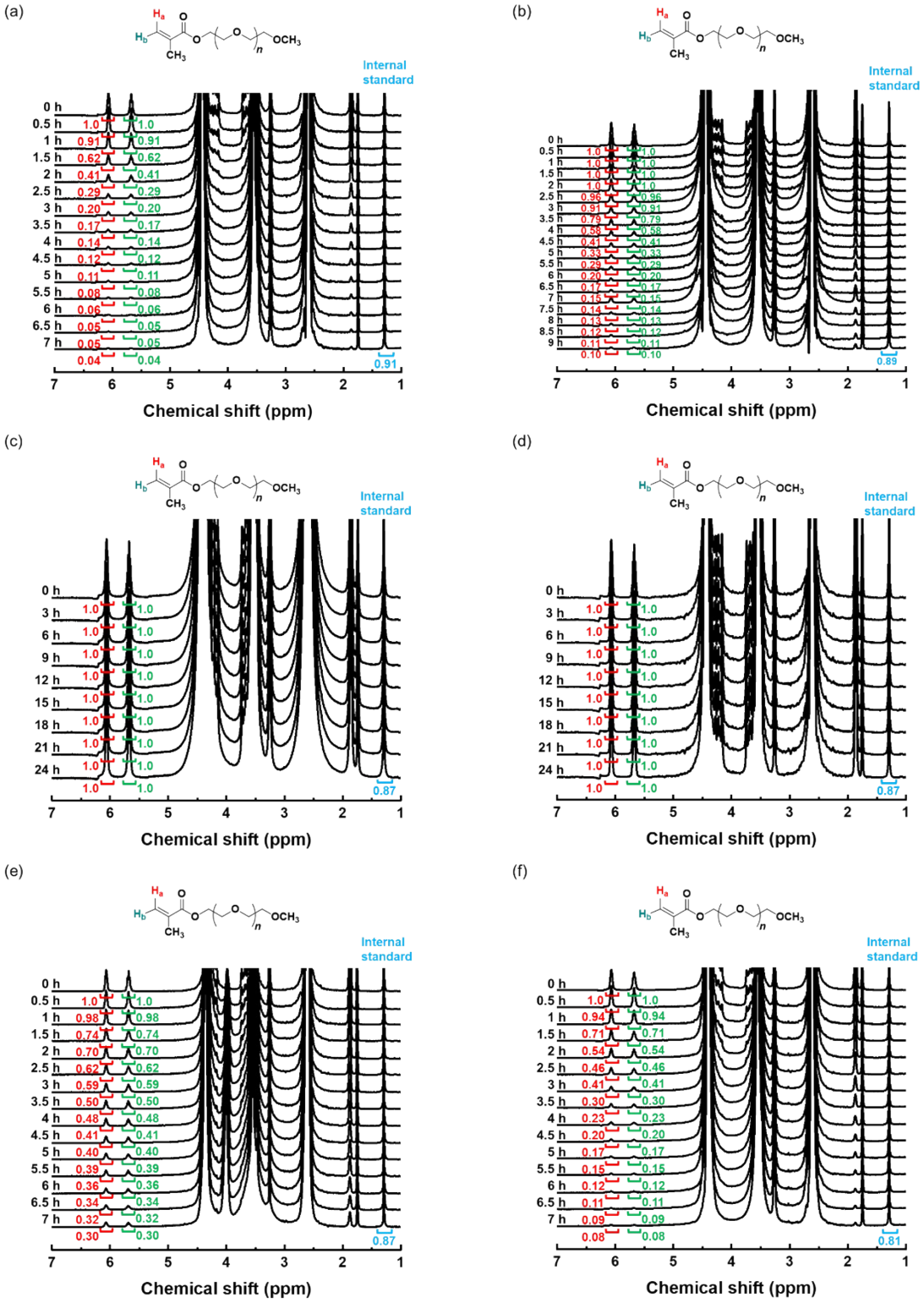

Fig. S48 ^{1}H NMR monitoring of OEGMA conversion, showing redrawn representations of the raw data from Table 2: (a) entry 13, (b) entry 14, (c) entry 15, (d) entry 16, (e) entry 17, and (f) entry 18.

References.

(1) H. Bader, V. Sturzenegger and J. Hoigne, *Water Res.,* 1988, **22**, 1109-1115.

(2) E. E. Wegner and A. W. Adamson, *J. Am. Chem. Soc.,* 1966, **88**, 394-404.

(3) (a) T. Zhang, J. Yeow and C. Boyer, *Polym. Chem*., 2019, **10**, 4653; (b) S. Shanmugam, J. Xu and C. Boyer, *Macromolecules*, 2017, **50**, 1832.

(4) M. Tanioka, A. Kuromiya, R. Ueda, T. Obata, A. Muranaka, M. Uchiyama and S. Kamino, *Chem. Commun.,* 2022, **58**, 7825-7828.